XIII. DESCRIPTION, TYPES, AND DISTRIBUTION OF MANGANESE NODULES

Tomoyuki Moritani, Shuji Maruyama, Masato Nohara, Yasumasa Kinoshita, Toshio Koizumi, and Tadashi Ito

Introduction

In the present GH77–1 cruise, manganese nodules were obtained from 31 stations among 37 total ones. Here we report the preliminary results of the observation mainly done during the time on-board the ship. Special attention was payed to confirming the applicability of the nodule type classification tentatively established in the previous GH76–1 cruise (MORITANI *et al.*, 1977), and to delineating the pattern of the nodule distribution and clarifying its relation to the geological factors, such as topography, surface sediment types, and substrate stratigraphy. In addition, a short description on the obtained rock samples from a few stations was included in this chapter for convenience' sake.

Method of nodule study

Bottom sampling was done at stations spaced over a distance of usually 1° or about 110 km apart, and in some areas they were set at the center of the usual grids or spaced more closely in case of the detailed survey. Two types of samplers used for were: the larger size grab, Okean (Ocean)-70, which can take a bottom portion of about 0.50 m^2 square area and 35 cm deep including both nodules and sediments; and the freefall photo grab sampler with about 0.13 m^2 catch area and only nodules or rocks in its hauls. The freefall photo grab sampler was dropped usually in two sets at each site of the Okean-70 grab sampling. Also, in some places, piston coring and sea bottom photographing by deep sea camera were made, always with the simultaneous bottom sampling by freefall photo grab.

Nodule samples obtained were described and studied on board for 1) observation of occurrence and morphology in and outside samplers, size classification, measurement of weight and calculation of abundance (kg/m^2); 2) photographing whole nodules of the freefall photo grab on the plate with a 5 cm grid scale; 3) observation of internal structures of the nodules on cut section; and 4) determination of mineral composition by X-ray diffractometer. Chemical analysis was carried out in the laboratory after the cruise as described in Chapter XI (MORITANI *et al.*, in this report).

The results are summarized in the sample lists (Table XIII–2) and photograph log (Fig. XIII–4). The relation of manganese nodules to the geological environment and chemical composition was examined by refering to other data of related studies, such as sedimentology, acoustic survey, and chemical analysis.

Types of manganese nodules

The morphological types were determined according to the classification schema of the

Table XIII–1 Morphological classification of manganese nodules (After MORITANI *et al.*, 1977).

Types	Size	Shape	Surface texture	MEYER (1973)	MAYLAN (1974)
Sr	small-medium	spheroidal/ellipsoidal	rough (granular or microbotryoidal)	Kr	s-m[S, E]r
SPr	small-medium	spheroidal/ellipsoidal/ intergrown	rough	Kr	s-m[S, E, P]r
SEr	medium-large	spheroidal/ellipsoidal	rough-botryoidal	B	m-1[S, E]r
Db	medium-large	discoidal/ellipsoidal	rough-botryoidal	B	m-1[D, D-E]r
Ss/SPs	small-medium	spheroidal/intergrown	smooth (smooth or microgranular)	Kg	s-m[P, S, E]s
DPs	small-medium	flattened/elongated/ discoidal/intergrown	smooth	Kg	s-m[D, P, E]s
ISs	large	irregular/spheroidal/ flattened/angular/fractured	smooth	G	1[S, F]s
IDPs	large	irregular/flattened/ discoidal/fractured	smooth		1[D, T, P, F]s
V	small-large	variable depending on the nucleus forms (Shark's teeth, nodule fragments etc.)	smooth or rough	KRU	s-m-1[B, F]r, s

Each type name is represented by the symbols taken from the initial of each morphological term, mostly applying the Meylan/Craig's classification method (MEYLAN, 1974). Here, each size class roughly corresponds in maximum diameter; small- < 4 cm, medium-4–6 cm, large- > 6 cm. Morphological symbols indicate; S-spheroidal, E-ellipsoidal, D-discoidal, P-poly or intergrown, I-irregular, V-variable, F-faceted, B-biological, T-tabular or flattened.

GH76–1 cruise samples as shown in Table XIII–1 (MORITANI *et al.*, 1977). This is based both on the surface structure, rough (r) or smooth (s), and on the shape, such as spheroidal (S), ellipsoidal (E), discoidal (D), intergrown or polylobate (P) and irregular (I) forms, and each type is represented by the combination of the initials of both terms as Sr or Ss/SPs. And then it contains nine types, such as Sr, SPr, SEr, Db, Ss/SPs, DPs, ISs, IDPs and V (variable).

The classification schema was proved to be applicable as a whole to this GH77–1 cruise samples. However, some slight differences were recognized between two cruise areas. One is that in the GH77–1 area the s (smooth) types predominated, and the occurrence of r (rough) types were rather limited both in numbers of stations and abundance. The other is that the GH77–1 cruise area is characterized by the predominance of larger size nodules than in GH76–1 area, particularly for s types. This partly seems to make it necessary or better to include some new types, such as Ss/SPs or separated Ss and SPs of larger size, into the schema, because Ss/SPs in the GH76–1 samples was originally for small-medium size. But, as the degree of difference between these nodules was permissible, and for avoiding the complication of the type names, even such samples were assigned to any of existing types of the classification.

In addition, in the GH77–1 area all samples in the same station area were of the similar type group, namely either r or s groups respectively, for example, including irregular (I) broken form and derived variable (V) fragments or in many cases as discoidal polylobate form (DPs).

The surface structures are likely to relate to the nodule occurrence in the water-sediment interface, namely either in exposed state (in case of s type) or in more buried one (in case of r type). Variations in shapes were proved to relate mostly to the inner structure or nucleus of nodules.

The results of identification of types for the nodule samples in each station are listed in Table XIII–2.

Distribution of manganese nodules

Two generalized maps were prepared to show the trend of the regional distribution of the manganese nodules and its ralations to the geological environment. Fig. XIII–1 shows the distribution of both abundance and types of all nodules, together with that of surface sediment types. Fig. XIII–2 represents a simplified distribution of nodule abundance in way of isopleth (iso-abundance line).

As for the local variation in nodule types and abundance in a limited station area, there were no marked differences among the data by two freefall photo grabs, Okean-70 grab and others. In each station area, nodule types and abundance were usually similar. A few exceptions were recognized for nodule abundance at two stations. At St. 707 the values vary from 0.2 or 3.9 to 10.9 kg/m^2, and at St. 711 the values range from zero or 0.2 to 15.4 kg/m^2. Although these exceptions indicate the possibilities of existence of more cases, the data based on the sampling at long distance of the order of 110 km apart seem to hold in showing the general tendency of nodule distribution.

As for the vertical distribution of nodules, the Okean grab sediment samples with about 35 cm thickness and coring samples show that the nodules occure almost in all cases in the water-sediment interface, in other words, on the surface of the bottom sediment

Table XIII–2 List of sampled and observed

The abundance in the parentheses shows the probably incorrect values due to the imperfect

Station no.	Sample no.	Associated sediment type [data by Okean-70G]	Morphological type	Total weight (kg)
701	FG33–1		Ss/SPs, DPs	0.50
	FG33–2		Ss/SPs, DPs, ISs	2.30
701A	G405	Deep sea clay	Ss/SPs	
702	G373	Deep sea clay	IDPs, V(crust)	4.92
	FG34–2		Ss/SPs, IDPs	1.56
705	G376	Siliceous clay	Sr	0.09
	FG37–1		Sr, SPr	0.04
	FG37–2		Sr	0.01
707	G378	Siliceous clay	SPr, Vr(slab)	1.95
	FG39–1		SPr, Vr(slab)	1.41
	FG39–2		SPr	0.03
708	G379	Deep sea clay	SPr, Sr	4.20
	FG40–1		SPr, Sr	0.39
	FG40–2		SPr, Sr	0.29
709	G380	Deep sea clay	DPs, IDPs	8.24
	FG41–1		DPs	0.37
	FG41–2		DPs	0.08
710	G381	Deep sea clay	DPs, Ss/SPs, IDPs	8.70
	FG42–1		DPs, Ss/SPs, IDPs	1.48
	FG42–2		DPs, Ss/SPs, IDPs	0.33
711	FG43–1		Ss/SPs, DPs	2.00
	FG43–2		Ss/SPs, DPs	0.03
712	G383	Deep sea clay	DPs, Ss/SPs, IDPs	10.56
	FG44–1		Ss/SPs, DPs, IDPs	1.27
	FG44–2		DPs, IDPs	0.25
713	G384	Deep sea clay	Sr, SPr	1.68
	FG45–1		Sr, SPr	0.38
	FG45–2		Sr, SPr	0.07
714	G385	Siliceous clay	Ss/SPs, DPs, IDPs	7.42
	FG46–1		Ss/SPs, DPs, IDPs	1.26
	FG46–2		Ss/SPs, DPs	0.18
718	G387	Deep sea clay	Ss/SPs, DPs	9.47
	FG48–1		DPs, Ss/SPs	2.28
	FG48–2		DPs, Ss/SPs, IDPs	2.67
719	G388	Deep sea clay	DPs, ISs, IDPs, Vs(n.f.)	11.84
	FG49–1		DPs, ISs, Vs(n.f.)	3.46
	FG49–2		DPs, IDPs, ISs, Vs(n.f.)	2.20
719A	FG71–1		ISs, IDPs, Vs(n.f.)	3.37
	FG71–2		ISs, IDPs, Vs(n.f.)	3.05
	FG71–3		DPs, IDPs	2.26
	FG71–4		DPs, Ss/SPs, IDPs	3.07
	FG71–5		DPs, ISs, IDPs	2.13
	FG71–6		DPs, ISs, IDPs, Vs(n.f.)	2.35
	FG71–7		DPs, IDPs, ISs, Vs(n.f.)	3.39
	FG71–8		ISs, IDPs, Vs(n.f.)	3.59

+ <0.1, ◇ 0.1–1.0, △ 1.0–5.0, ▲ 5.0–10.0, ○ 10.0–20.0, ● >20.0 kg/m²

manganese nodules of GH77–1 cruise.
sampling, judged from the sea bottom photograph data by freefall photo grab sampler.

Abundance		Number of size fraction (mm)							Bulk wet	Inner structure
	(kg/m²)	>10	10–8	8–6	6–4	4–2	2–1	<1	density (g/cm³)	nucleus etc.
(△)	(3.8)				5	36	24			Nodule fragment, clay, altered rock, shark's teeth
○	17.7			3	12	95	63			
(▲)	(7.1)				31	152	89			
▲	9.8	6	3	12	13	8				Clay, altered rock
○	12.0		1	1	13	39	19			
◇	0.2					5	2			Shark's teeth, pumice, fossil bone
◇	0.3					3	1	6		
+	<0.1						3	2		
△	3.9	1	2	3	12	102	100		2.0	Clay
○	10.9		2	4	10	53	19	45		
◇	0.2						15			
▲	8.4		3	9	29	106	112			Clay
△	2.9				1	24	88			
△	2.2				1	13	28			
○	16.5			10	120	80			2.0	Clay, shark's teeth
(◇)	(0.5)				4	23				
(△)	(2.8)				2	2				
○	17.4			3	53		107		2.1	Clay, many of smaller nodules lack heterogeneous cores.
○	11.4				3	109	362			
△	2.5					20	62			
○	15.4				8	172	130			Many lack heterogeneous cores.
◇	0.2						6			
●	21.1			11	134	283	1		1.6	Cherty rock, clay, many lack heterogeneous cores.
○	11.3			5	19	59	9			
(△)	(1.9)		1	11						
△	3.4					128	251		2.0	Clay
△	2.9				2	13	39			
◇	0.5					4	13			
○	14.8			6	58	298	44		2.0	Clay
▲	9.7				11	48	6			
(△)	(1.4)				1	12	1			
○	18.9		3	17	121	157	11		1.9	Clay
○	17.5			5	19	39				
●	20.5			7	24	46				
●	23.7			12	76	>300				Clay, altered rock
●	26.6			3	22	77			2.1	
○	16.9			2	10	47				
●	25.9			7	32	73				Clay, some altered rock, some lack heterogeneous core.
●	23.5			4	24	54				
○	17.4			5	35	67				
●	23.6			6	36	45				
○	16.4			5	33	58				
○	18.1			25	71	3				
●	26.1		3	5	31	58				
●	27.6			6	26	73				

Table XIII-2

Station no.	Sample no.	Associated sediment type [data by Okean-70G]	Morphological type	Total weight (kg)
720	G389	Siliceous clay	Ss/SPs	1.82
	FG50-1		Ss/SPs	0.85
	FG50-2		Ss/SPs	0.53
721	G390	Calcareous-siliceous clay	DPs, Vs(n.f.)	0.68 (+1.30)
	FG51-1		DPs, Vs(n.f.)	0.96
	FG51-2		DPs, Vs(n.f.)	0.61
722	G391	Siliceous clay	IDPs, DPs, Vs(n.f.)	9.96
	FG52-1		IDPs, DPs, Vs(n.f.)	3.65
	FG52-2		IDPs, DPs, Vs(n.f.)	3.07
722A	D212		IDPs, DPs, Vs(n.f.)	180.
723	G392	Deep sea clay	Sr, SEr	0.52
	FG53-1		Sr	0.18
	FG53-2		Sr, SPr	0.32
724	G393	Deep sea clay	Sr, SPr	0.26
	FG54-1		Sr, SPr	0.07
	FG54-2		Sr, SPr	0.06
725	G394	Deep sea clay	Sr, Db, Vr(slab)	3.83
	FG55-1		SPr	0.01
	FG55-2		Sr, SPr	0.01
727	G397	Deep sea clay	Sr	0.31
728	FG60-1		Sr	0.08
	FG60-2		Sr	0.15
729	FG61-1		Ss/SPs, IDPs	3.31
	FG61-2		Ss/SPs	2.51
730	FG62-1		SPr, Sr	1.49
	FG62-2		SPr, Sr	1.26
732	FG64-1		Sr	0.01
	FG64-2		Sr	0.01
733	FG65-1		ISs, DPs, IDPs, Vs(n.f.)	2.81
	FG65-2		ISs, DPs, IDPs, Vs(n.f.)	3.15
733A	D211		ISs, IDPs, DPs, Vs(n.f.)	300.
734	FG66-1		Sr, SEr, SPr	1.41
	FG66-2		Sr, SPr, SEr	0.75
735	FG67-1		ISs, DPs, Vs(n.f.)	3.61
	FG67-2		ISs, DPs, Vs(n.f.)	1.55
736	FG68-1		DPs, Ss/SPs	3.56
	FG68-2		DPs, Ss/SPs	3.45
737	FG69-1		ISs, DPs, Vs(n.f.)	3.07
	FG69-2		ISs, DPs, Vs(n.f.)	3.39
738	G402	Deep sea clay	ISs, DPs, Vs(n.f.)	6.98
	FG70-1		ISs, DPs, IDPs	1.89
	FG70-2		ISs, IDPs, DPs	3.41
739	G403	Deep sea clay	Ss/SPs	not determined
	FG72-1		DPs, Ss/SPs	2.42
	FG72-2		IDPs, DPs, ISs	2.13

+ <0.1, ◇ 0.1–1.0, △ 1.0–5.0, ▲ 5.0–10.0, ○ 10.0–20.0, ● >20.0 kg/m²

(Continued)

Abundance		Number of size fraction (mm)							Bulk wet density (g/cm^3)	Inner structure nucleus etc.
	(kg/m^2)	>10	10–8	8–6	6–4	4–2	2–1	<1		
△	3.6				5	116	99	55		
▲	6.5				3	51	61	19		
△	4.0				1	25	32	22		
○	16.4				21	233	272		2.0	Clay, many lack heterogeneous cores.
▲	7.4				2	52	35			
△	4.7					34	52			
○	19.9			8	99	189				
●	28.1			5	37	42			2.0	
●	23.5			1	34	42				
△	1.0				4	25	28		2.0	Pumice
△	1.4					10	12			
△	2.5					23	24			
◇	0.5					11	72	159	2.0	Shark's teeth
◇	0.6					2	18	44		
◇	0.5					3	24	23		
▲	7.7	3	4	1	15	91	78		1.9	Pumice, altered volcanic rock, cherty rock, shark's teeth
+	<0.1						1			
+	<0.1						4			
◇	0.6					18	51	>300		
◇	0.6					1	22	26		
△	1.2					2	38	30		
●	25.5		1		32	42				Clay, altered rock
○	19.3				3	53	12			
○	11.5			2	27	40	3			Clay
▲	9.7			4	16	38	5			
+	<0.1						1			
+	<0.1						3			
●	21.7			2	18	37	5			Clay, many lack heterogeneous cores.
●	24.2			11	23	22				
○	10.9				14	48	14	3		Clay
▲	5.8				6	12	31	10		
●	27.7			10	20	60	2			Clay, some lack heterogeneous cores.
(○)	(11.9)			1	9	41	10			
●	27.4			2	16	42	3			Clay
●	26.5				23	67				
●	23.6			7	15	13				
●	26.1			11	17	24				
○	14.0			6	55	98			2.0	Clay
○	14.6	1	2	1	17	16				
●	26.2			8	27	31				
	?									Altered rock
○	18.6			7	143	44				
○	16.4				29	53	3			

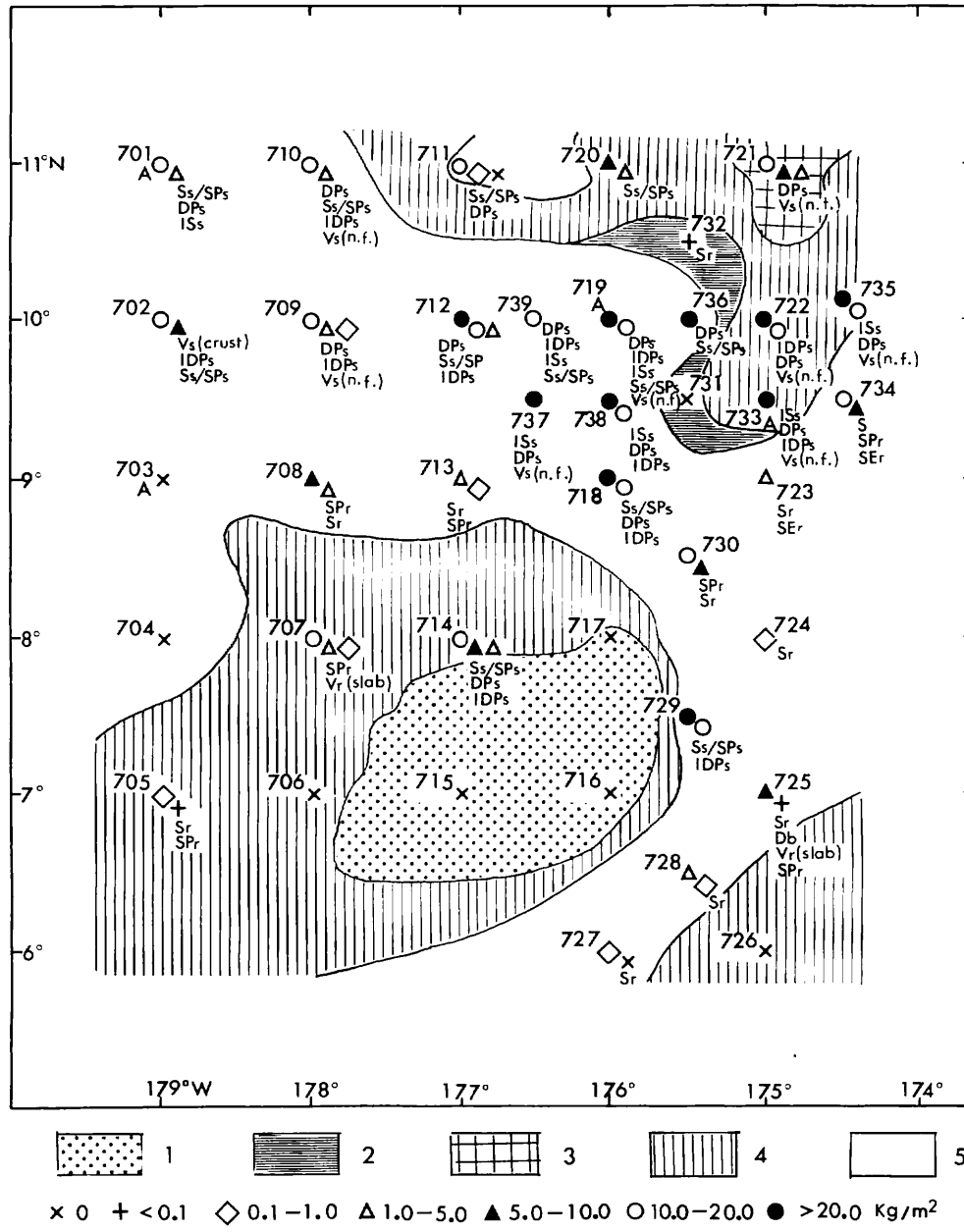

Fig. XIII–1 Generalized map of distribution of surface sediments, manganese nodules and their abundance. Abundance is shown in kg/m², and two or three different marks of it in one station indicate variation of its values according to the different sampling points within the same station area. Surface sediment data are after NAKAO (Chap. IX, in this report): 1) Calcareous ooze; 2) Siliceous ooze; 3) Calcareous-siliceous clay; 4) Siliceous clay; 5) Deep sea clay.

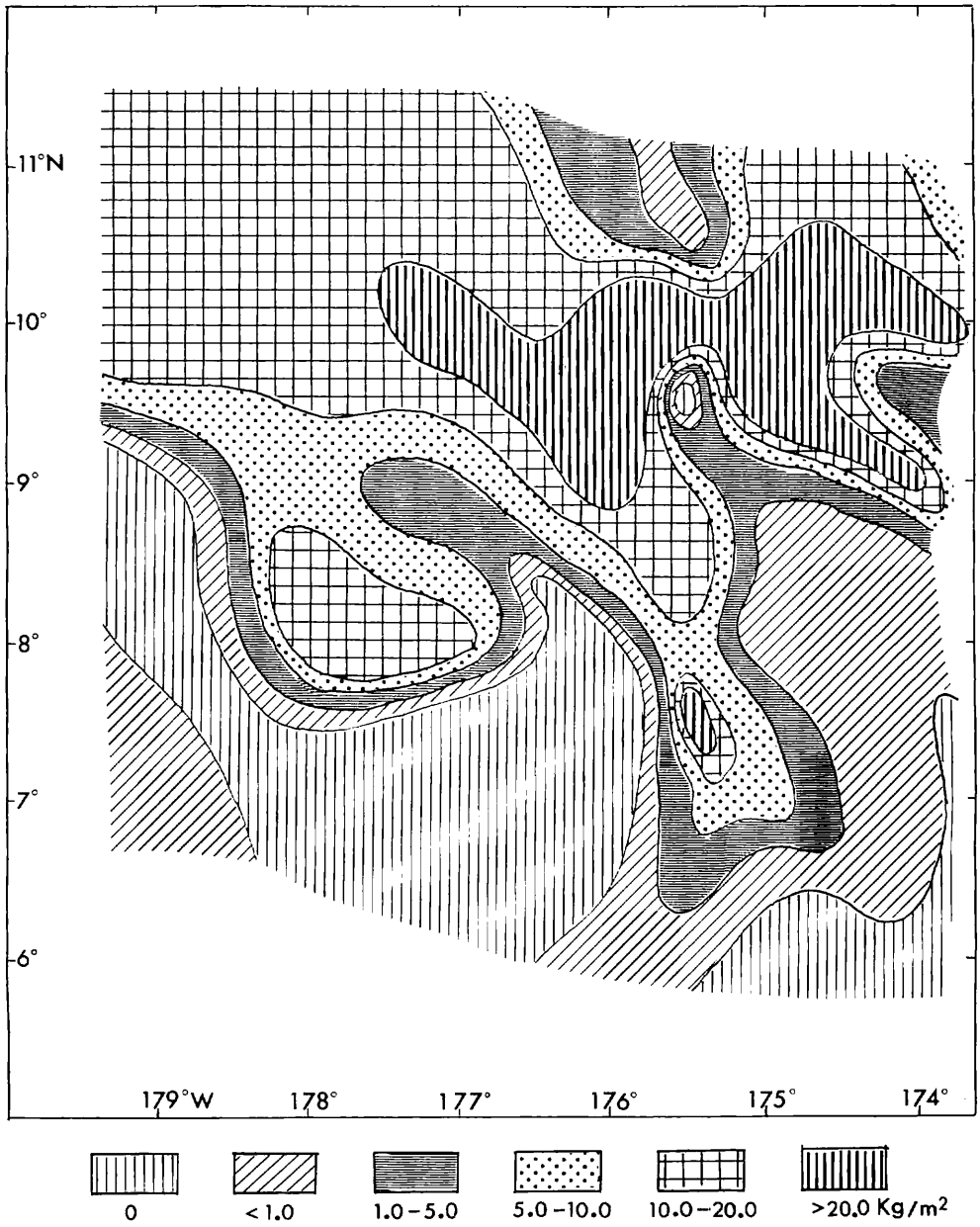

Fig. XIII–2 Distribution of manganese nodule abundance. The unit is in kg/m². This map shows only the general trend basing on the data from roughly spaced sampling stations.

column. One exception was recognized at St. 721, where some nodules occurred buried within the sediment column, but the type was of the same one as the surface nodules, in this case, of DPs type.

As shown in abundance distribution map (Fig. XIII–2), the manganese nodules are distributed not uniformly but with clear trend. Namely, the high abundance area lies markedly in the northern belt zone, and partly to the east foot of the Magellan Rise, while the barren area is extensive towards the southern part of the survey area including the Magellan Rise.

This regional features of the nodule distribution seem firstly to relate to the regional submarine topography of the survey area. As a whole, the northern high abundance area lies in the abyssal zone at a depth of 5,000–6,000 m, between two topographic highs, the Northern Seamounts at a depth of 4,500 m and the southern Magellan Rise at a depth of 3,500 m. Besides, the northern high nodule abundance area is characterized by a rather ragged topography with predominant deep sea hills, differing from other parts of the abyssal area.

These regional topographic features are reflected on the sediment types, acoustic stratigraphical features, and sedimentation history as a whole. The topographic highs, particularly of the Magellan Rise are area of high sedimentation rate because they stand above the calcium carbonate compensation depth of around 4,500 m. The abyssal areas of the southern part with thick acoustic transparent layer of Type A or Type C (acoustic turbidites) of Unit I layer are represented also by high sedimentation environment presumably influenced by the high biogenic productivities of the equatorial zone.

However, as the zone with such thick acoustic layer of Type C is also developed along the northern area adjacent to the high nodule abundance area supposedly in the similar condition as for biogenic productivities, another factors such as submarine topography and bottom current regime may have influenced the sedimentation rate. Namely, the high nodule abundance area characterized by the predominant deep sea hills and thin acoustic transparent layer less than 50 m in thickness may have been affected by relatively stronger bottom current.

Thus, it is concluded that, generally speaking, manganese nodules are distributed more abundantly in the lower sedimentation rate area, which may be represented as the total effects of topographic condition, biogenic productivities or sediment supply, and bottom current regime, meaning lesser diluting effect by the sediments on the nodule formation. However, even there have been such regional conditions, the nodule distribution is still variable, and in some cases, the high abundance is sporadically distributed, and then some local metal supply itself may have contributed to the nodule formation.

Description of obtained rock samples

Along the foot and northern environs of the Magellan Rise, rock samples of basalt, chert, and phosphorite were sampled by Okean-70 grab and freefall grab (Sts. 702, 706, and 711).

Basalts obtained from St. 706 (Fig. XIII–3) range in size from 5 cm to 20 cm, and are of columner or angular shape. The surface of these samples is coated by thin manganese oxide layer. Many vesicules observed on the cut section suggest that the basalt exposed and solidified near the sea bottom surface. Though the whole texture remains fairly fresh,

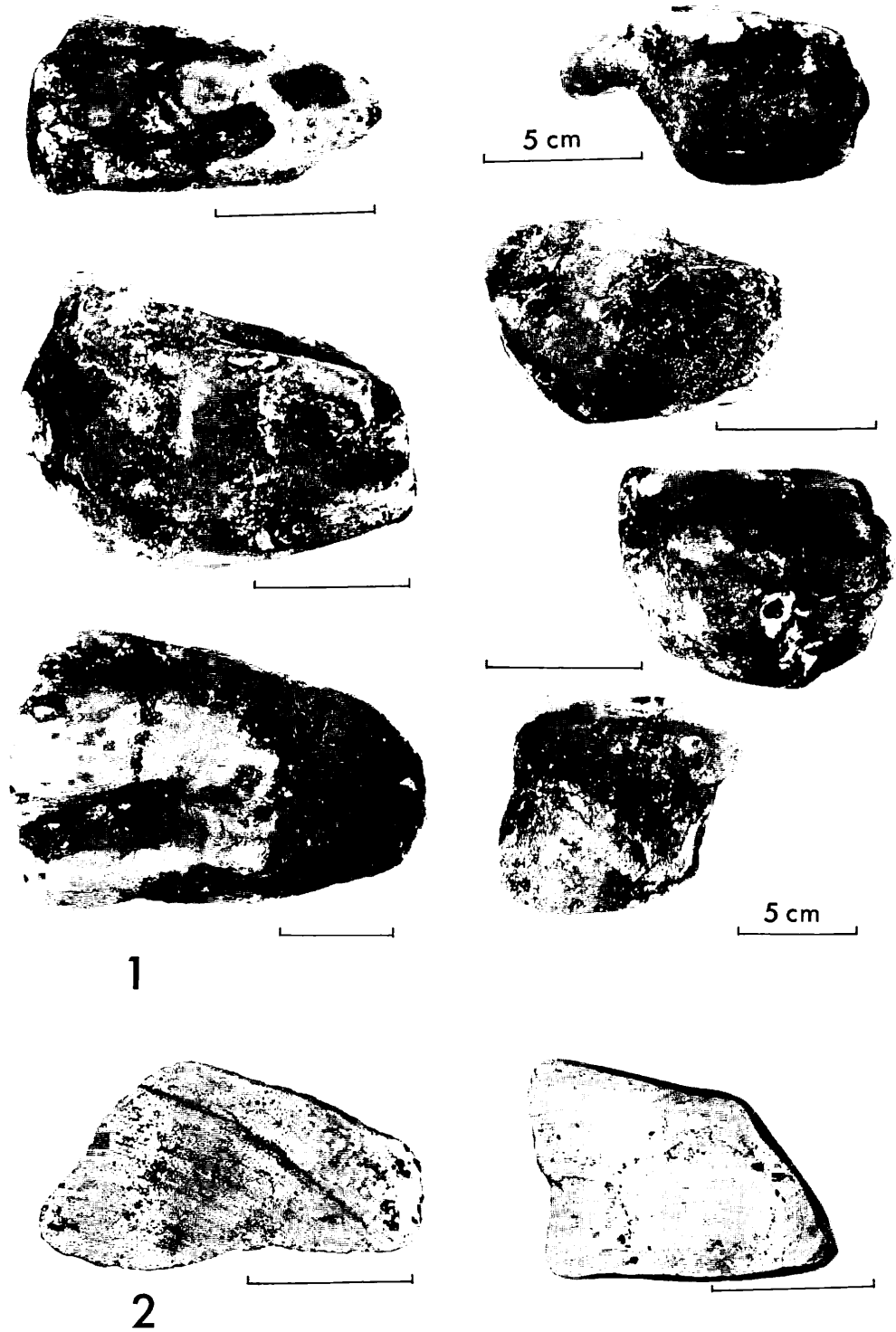

Fig. XIII-3(A) Photographs of sampled basaltic rocks (St. 706–G377). 1: Whole rock fragment; 2: Cut section.

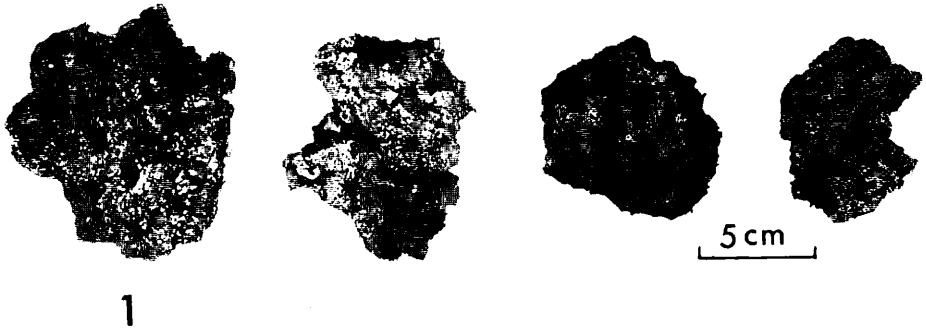

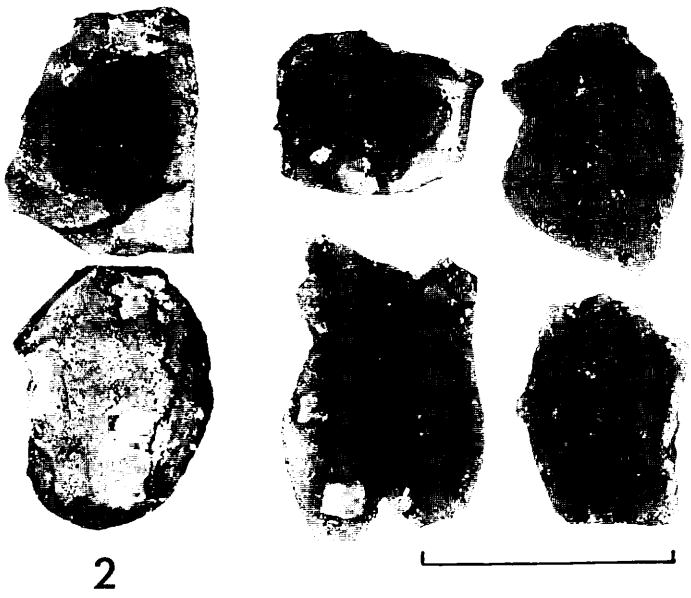

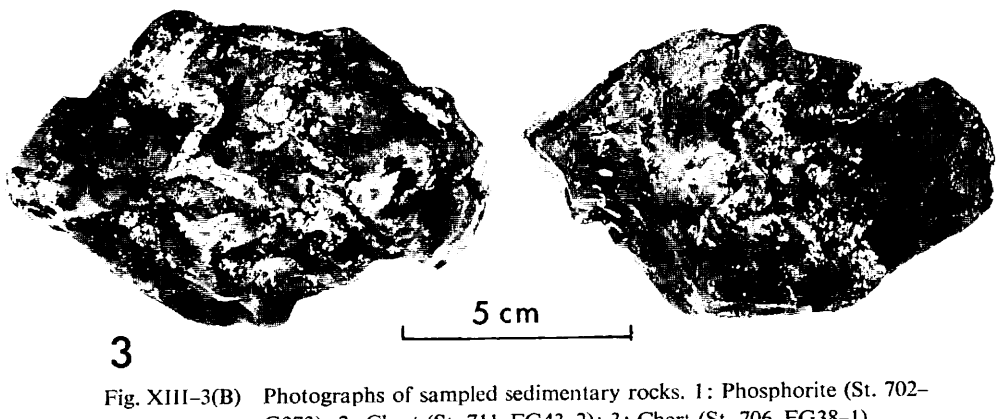

Fig. XIII-3(B) Photographs of sampled sedimentary rocks. 1: Phosphorite (St. 702–G373); 2: Chert (St. 711–FG43–2); 3: Chert (St. 706–FG38–1).

Fig. XIII-4(1-30) Photograph log of manganese nodules from each station. Whole free-fall grab samples were photographed on a plate marked with a unit square catch area of 33.5 cm×33.5 cm=0.13 m^2 of the freefall grab sampler. Photographs of typical samples both of freefall grab and Okean-70 grab were taken on the 5 cm grid scale.

ST.701 FG33−1

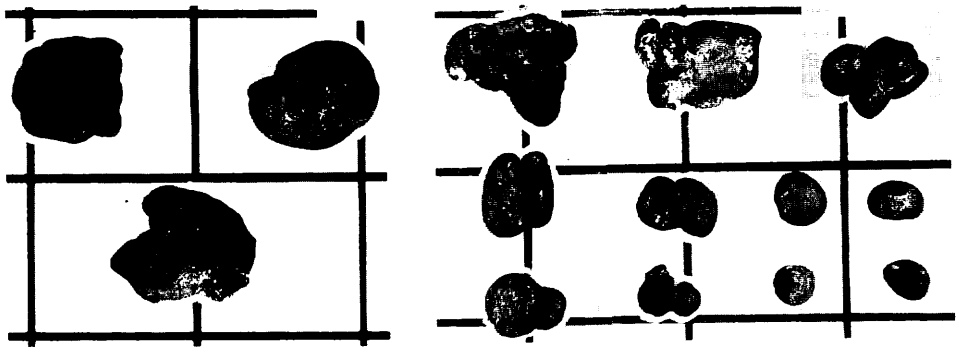

FG33−2

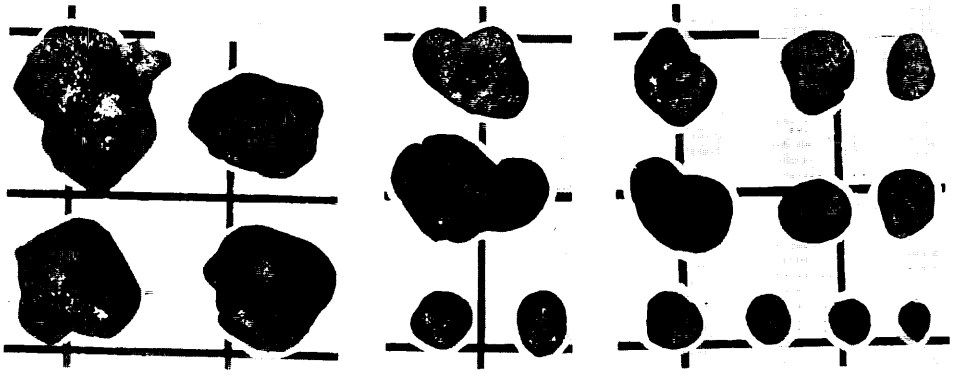

G405

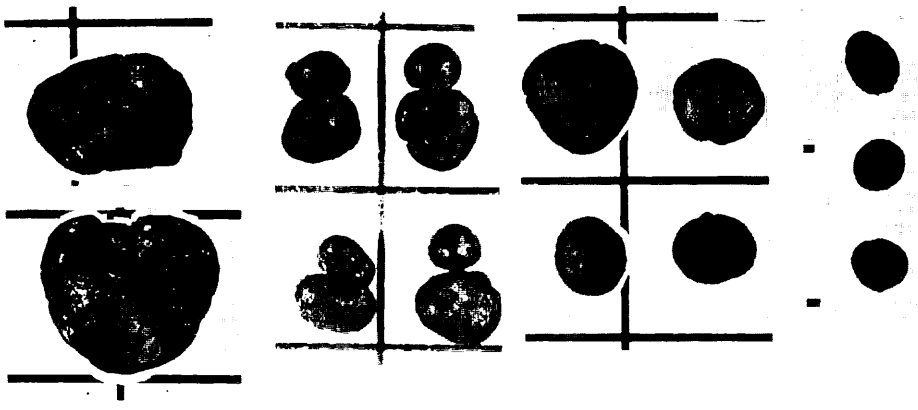

ST.702 FG34−2

G373

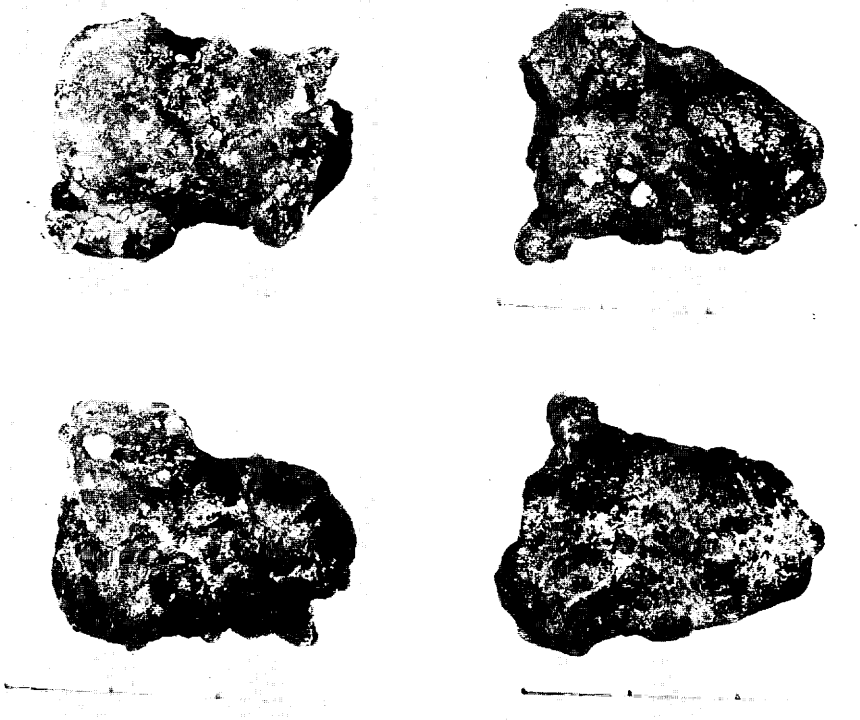

(2)

ST.707 FG39-1

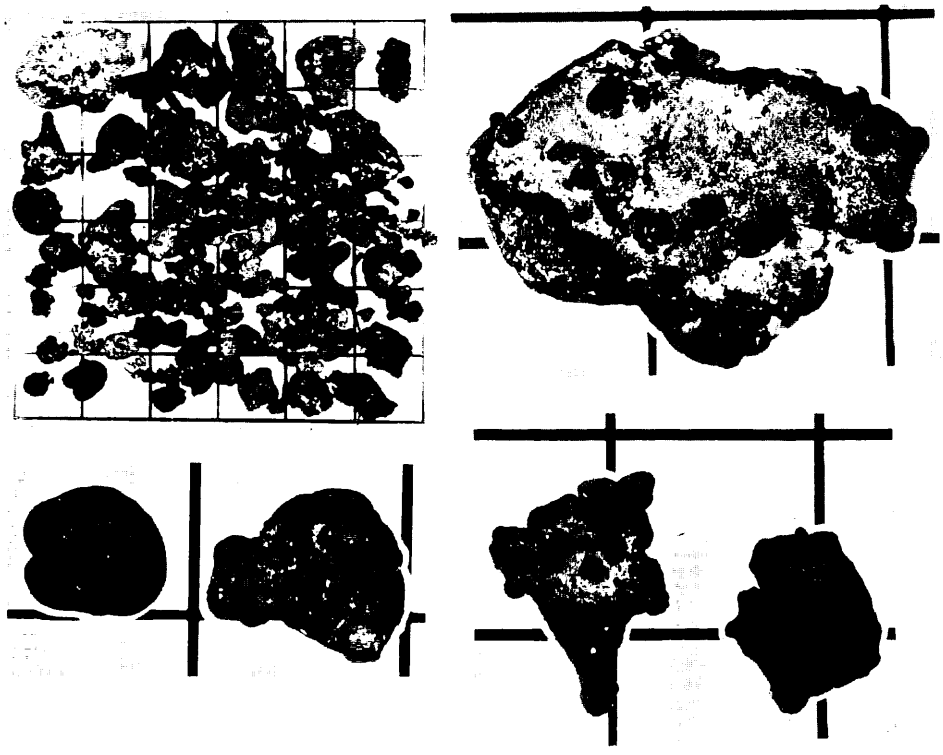

G 378

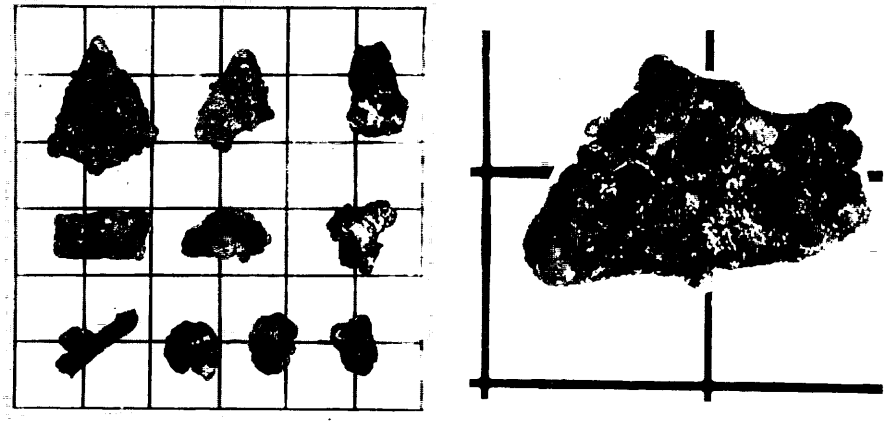

ST.708 FG40−1

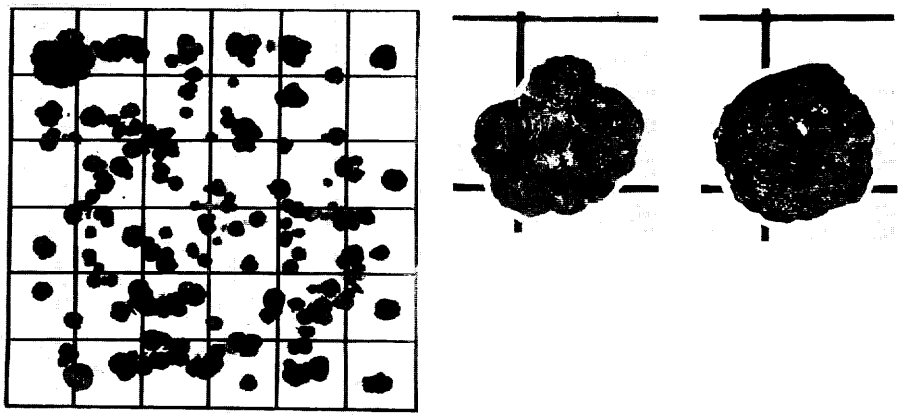

FG40−2

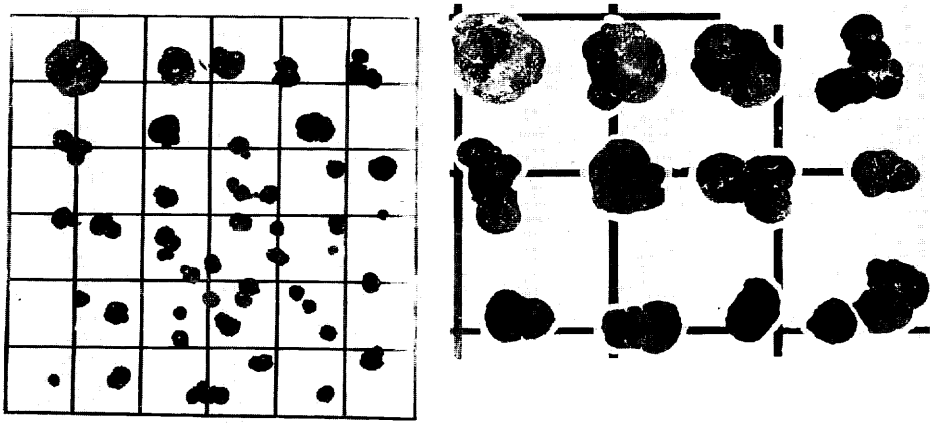

G379

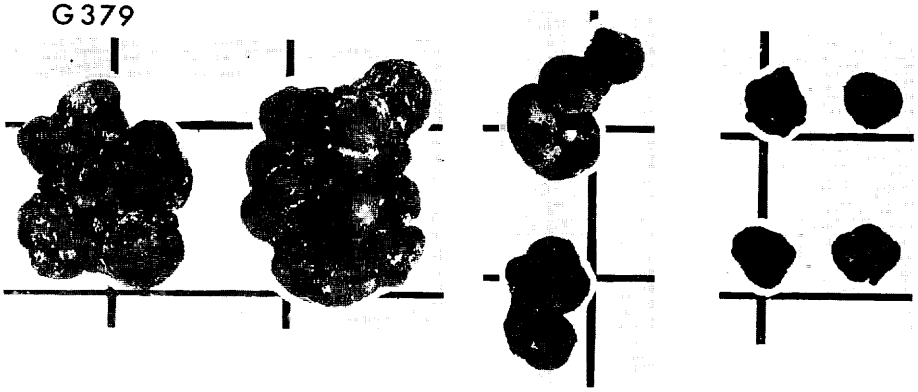

(4)

ST.709 FG41−1

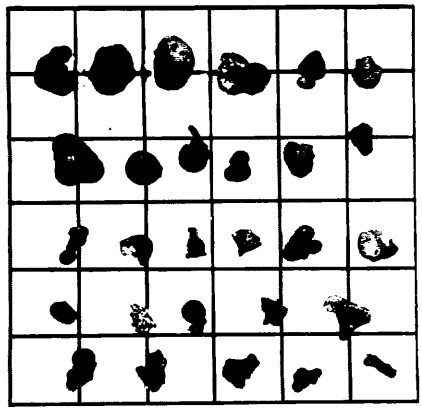

FG41−2

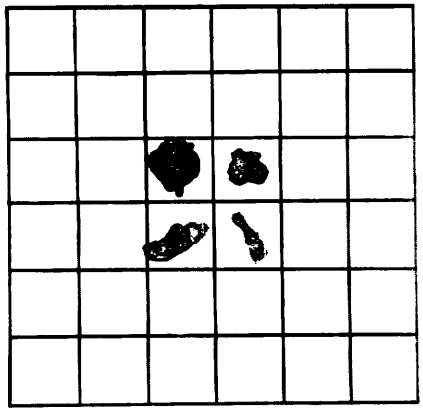

G380

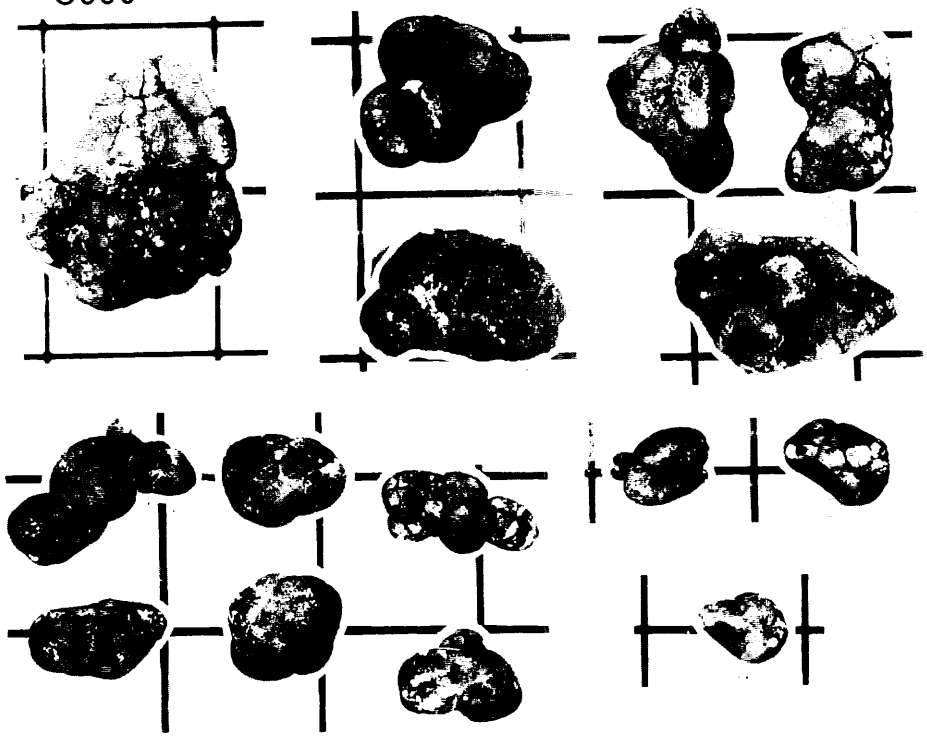

ST.710 FG42−1

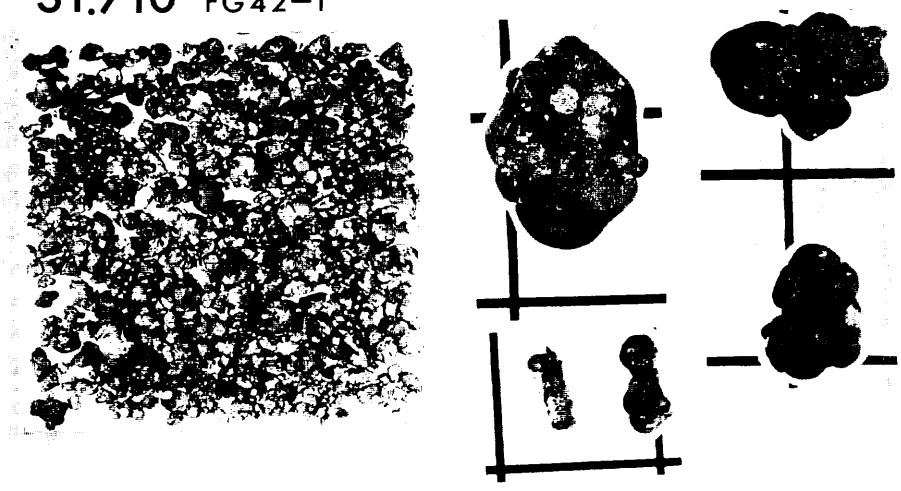

FG42−2

G381

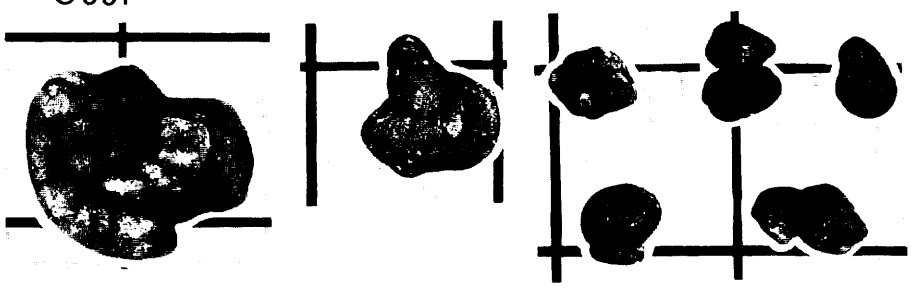

(6)

ST.711 FG43−1

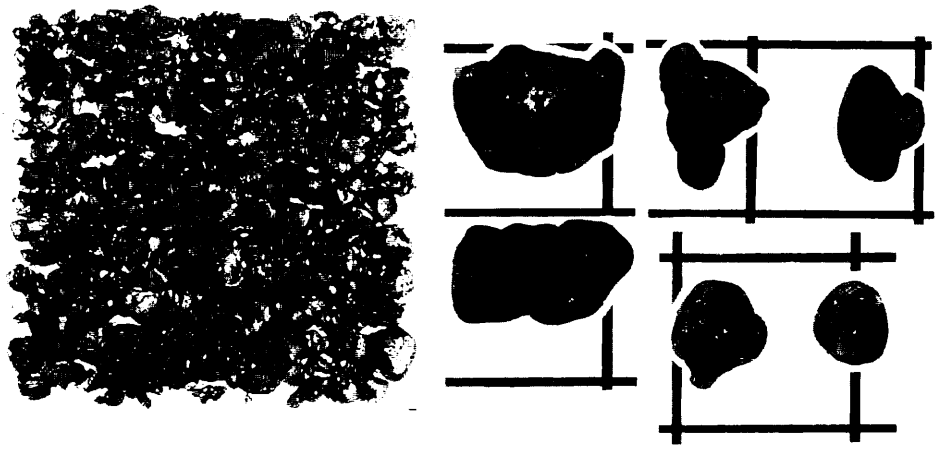

FG43−2

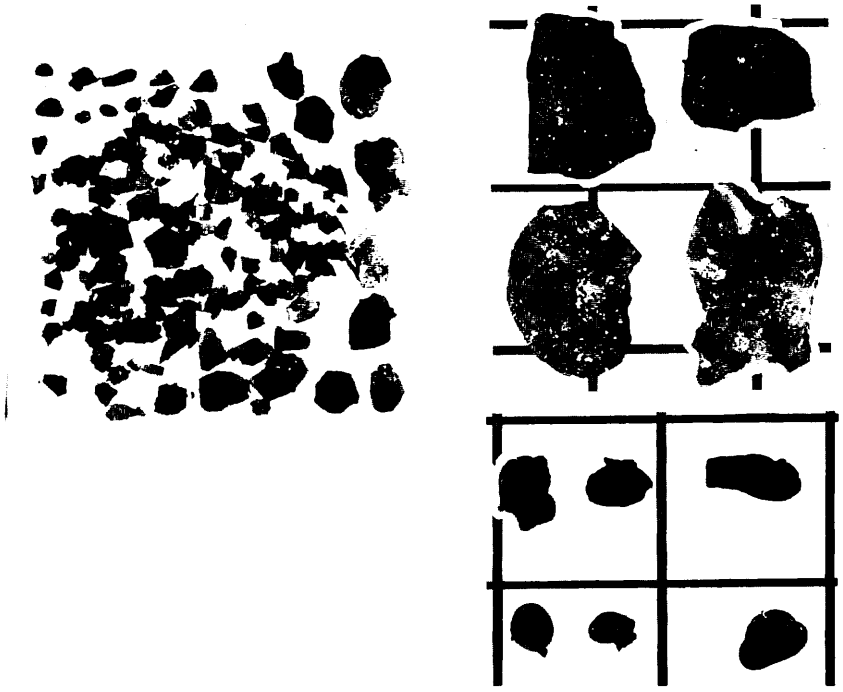

ST.712 FG44−1

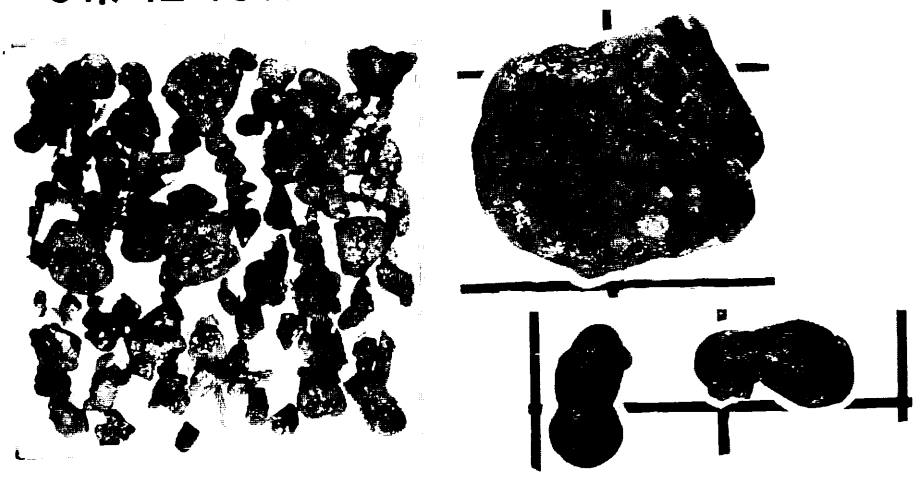

FG44−2

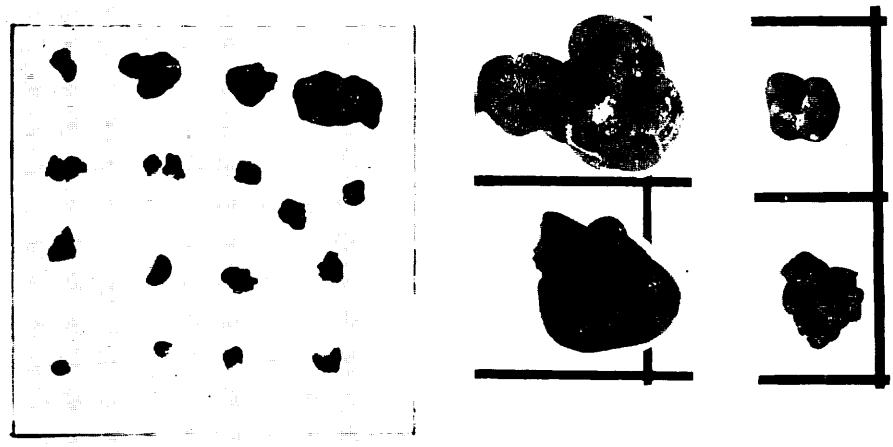

G383

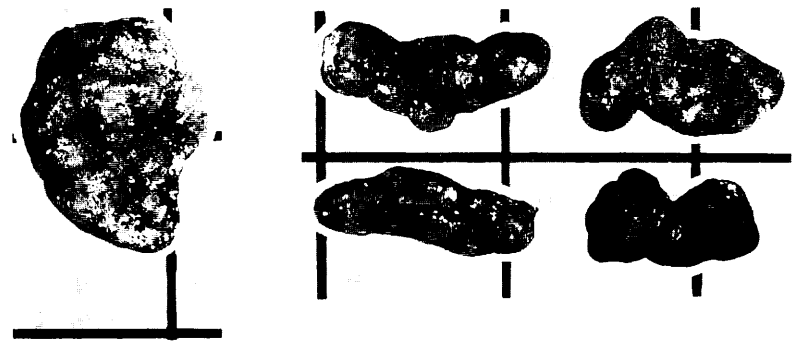

(8)

ST.713 FG45—1

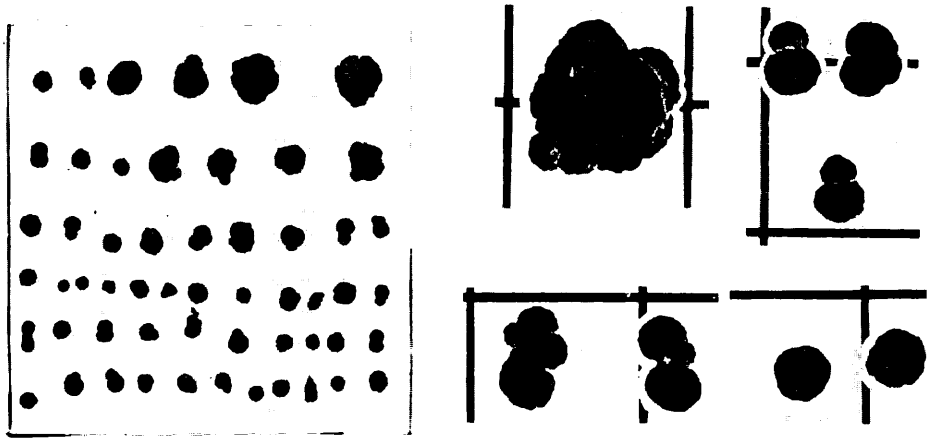

FG45—2

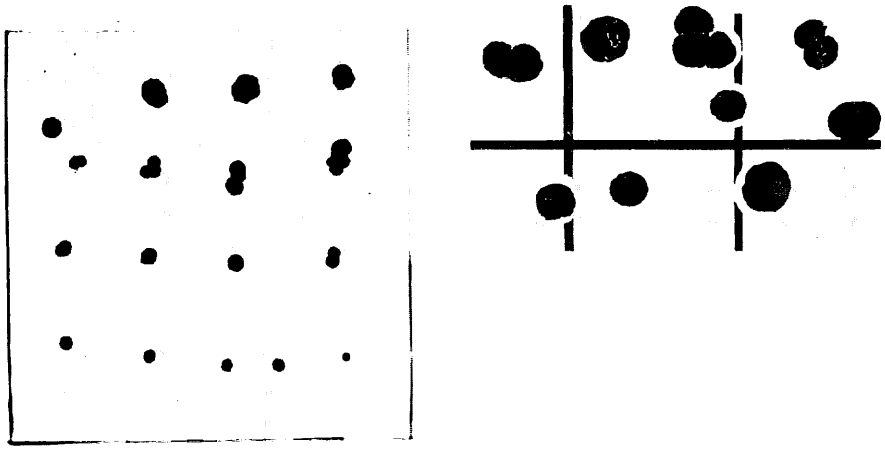

G384

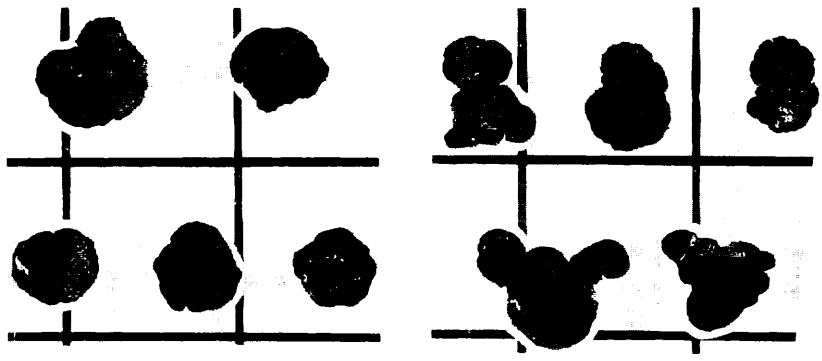

(9)

ST.714 FG46–1

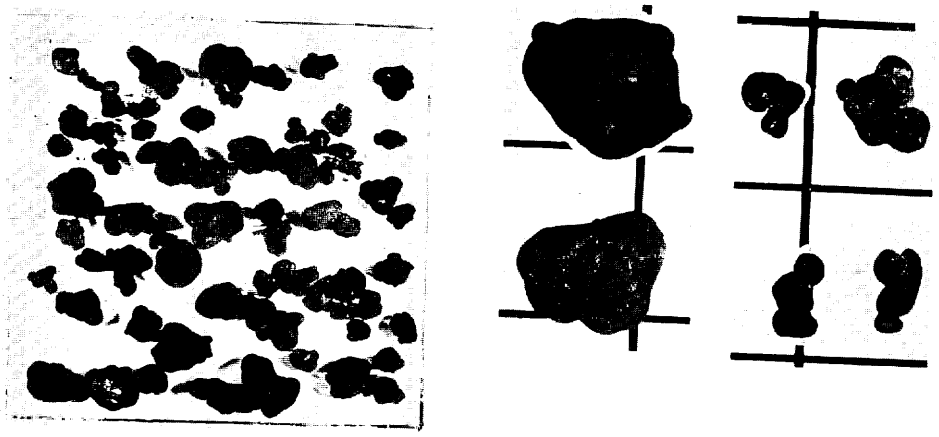

FG46–2

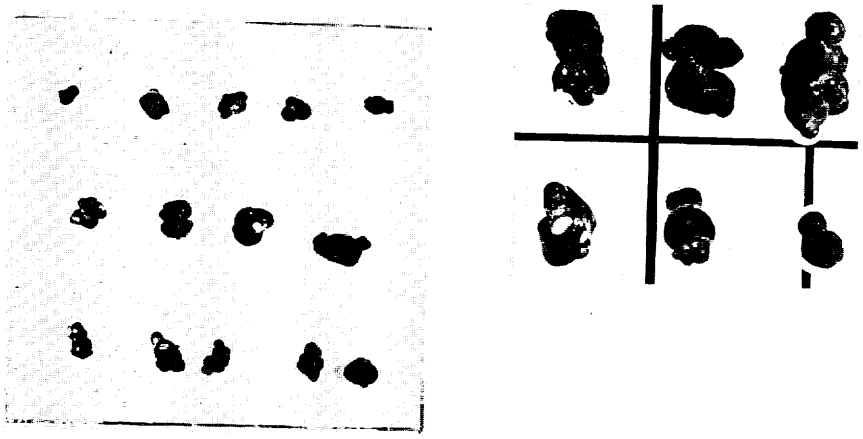

G385

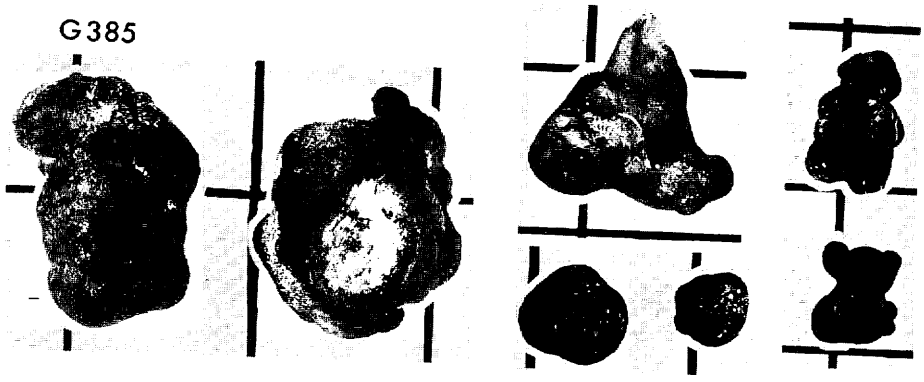

(10)

ST.718 FG48−1

FG48−2

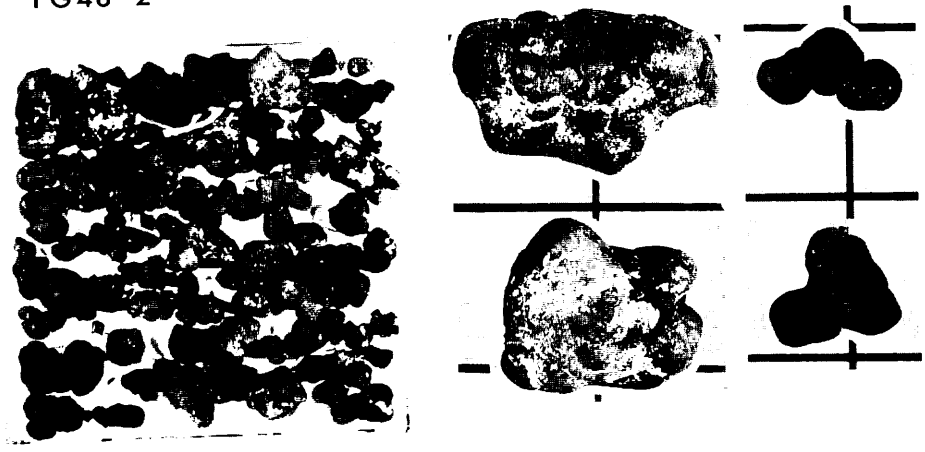

G387

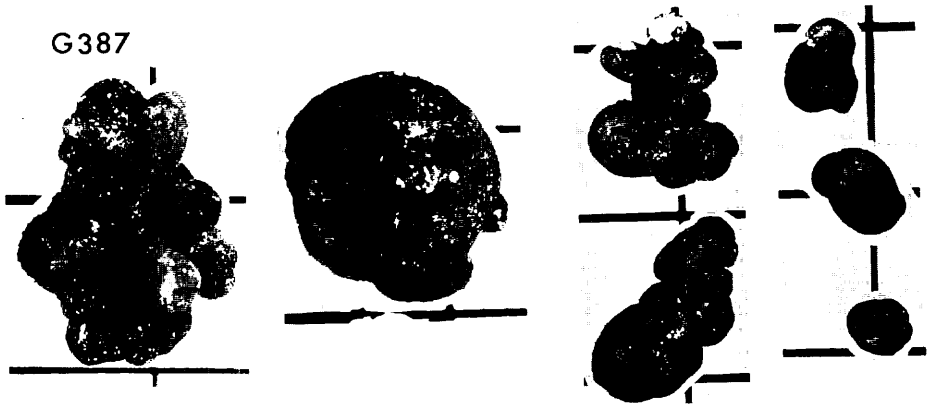

ST.719 FG49−1

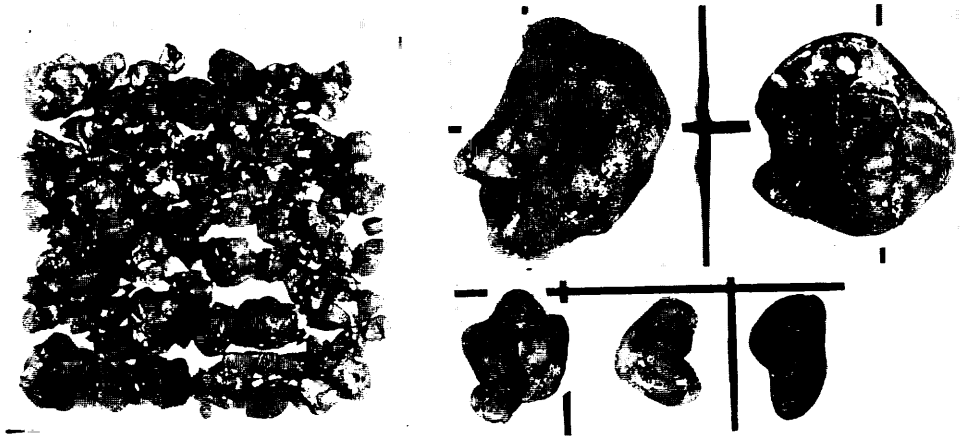

FG49−2

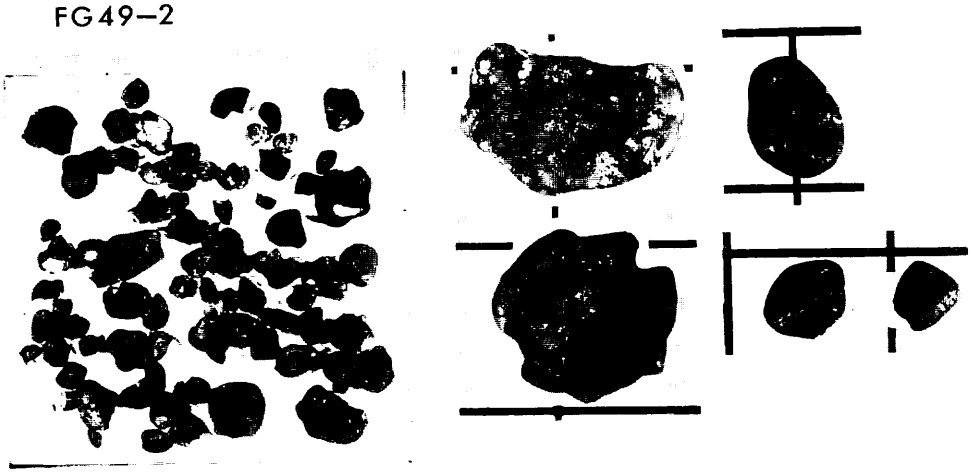

G388

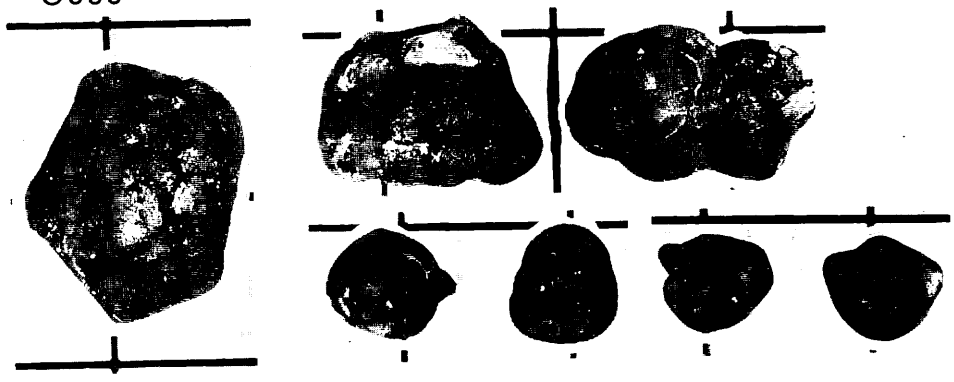

ST.719A FG71–1

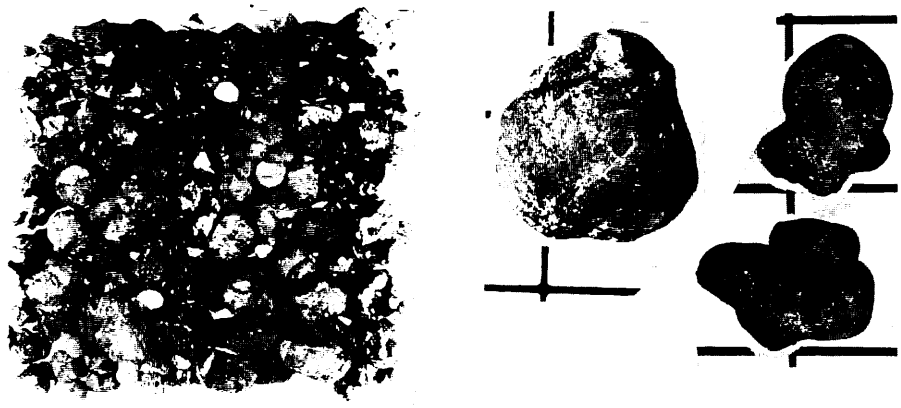

FG71–2

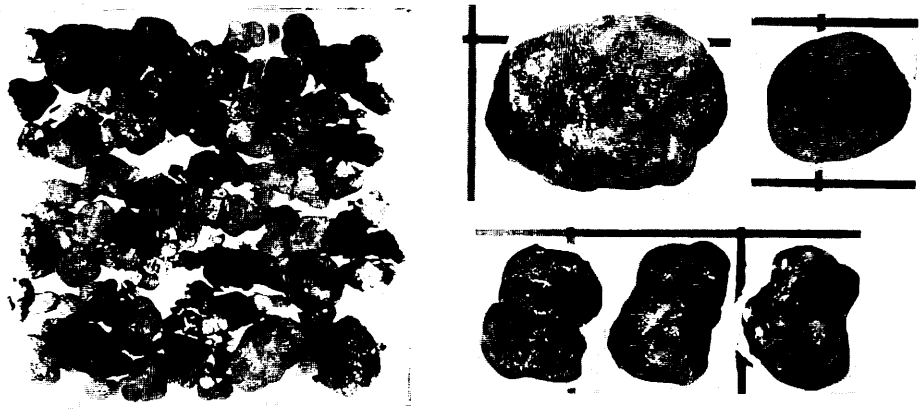

FG71–3

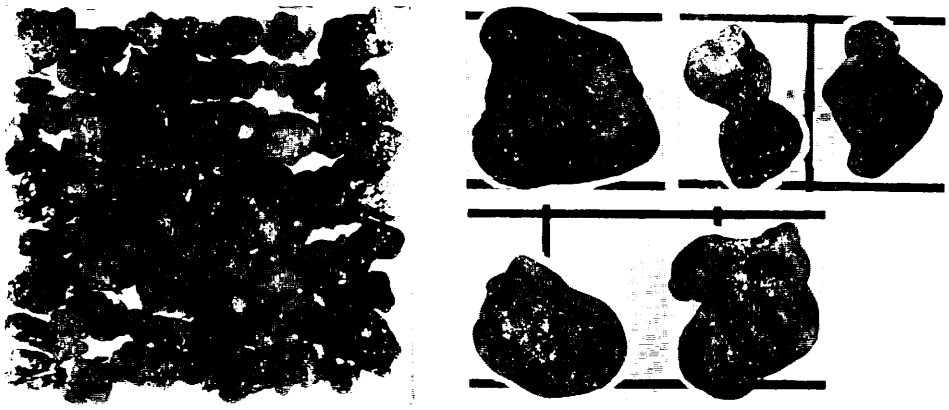

FG71−4

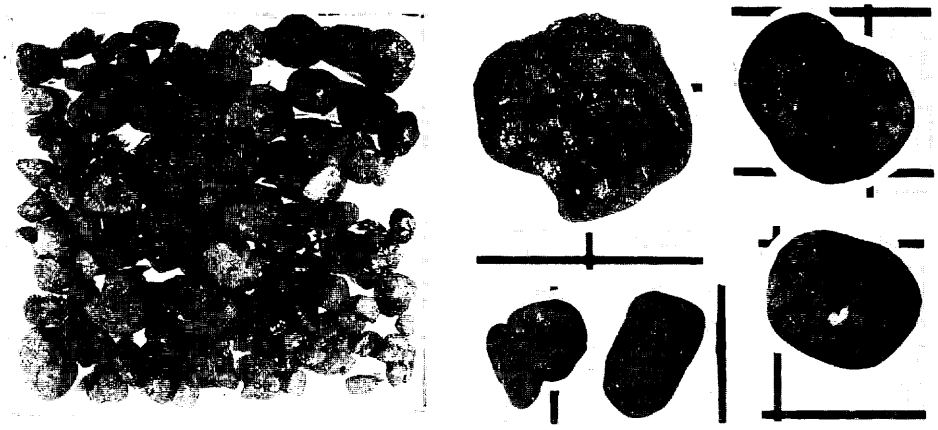

FG71−5

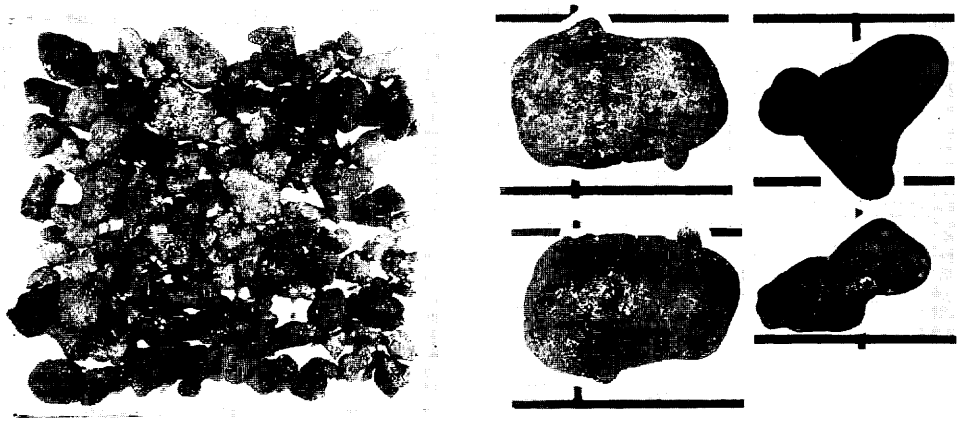

FG71−6

FG71–7

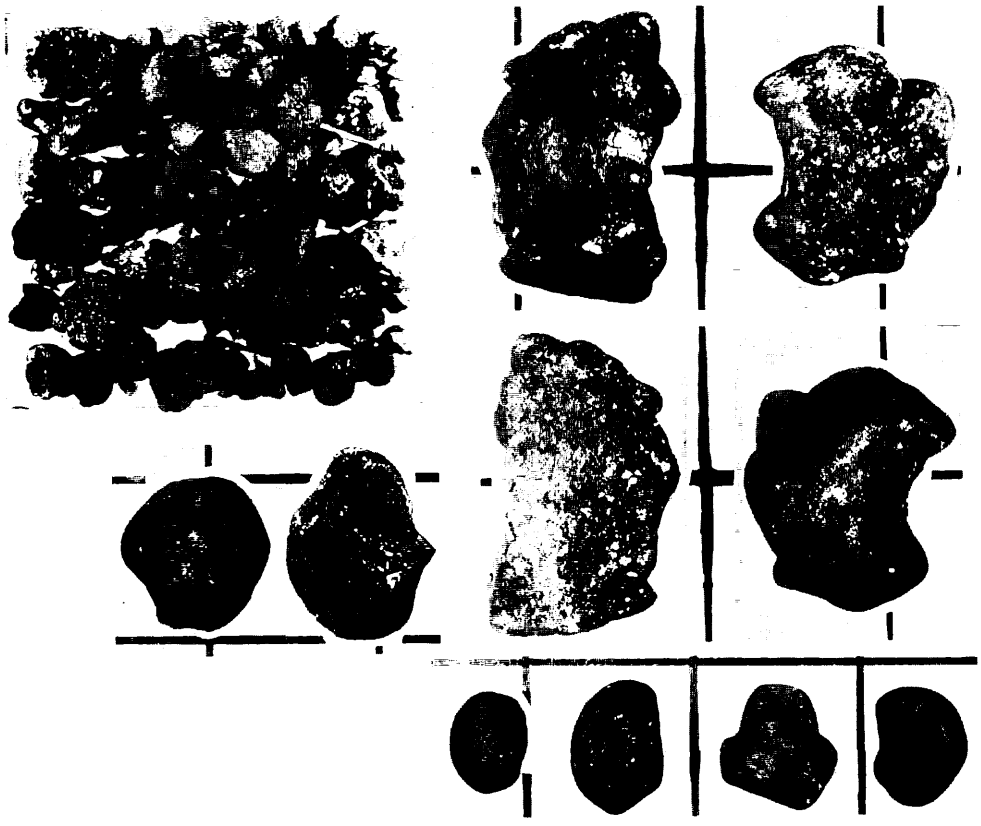

FG71–8

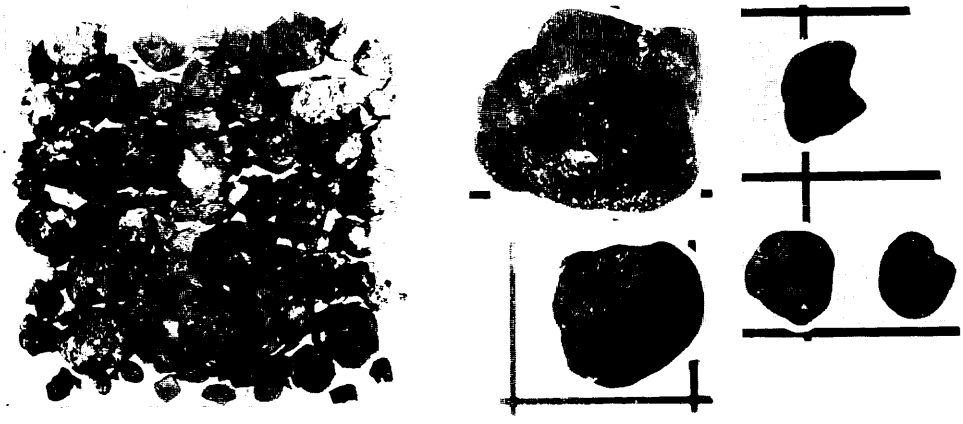

ST.720 FG50−1

FG50−2

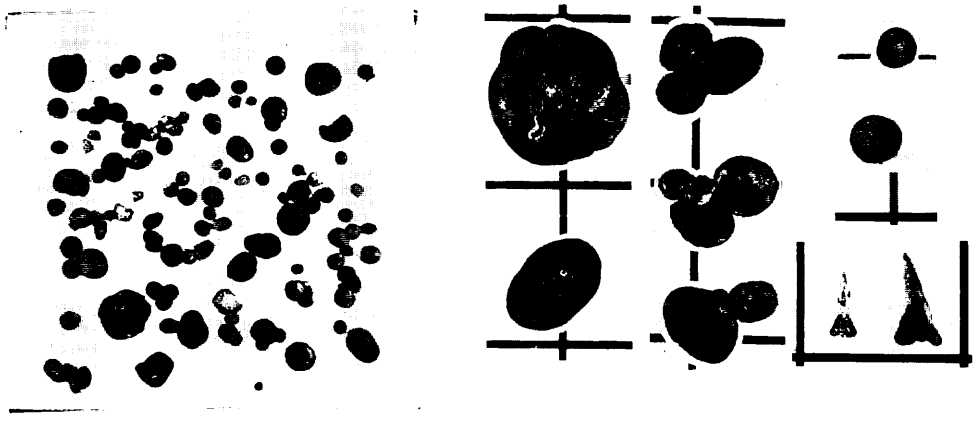

G389

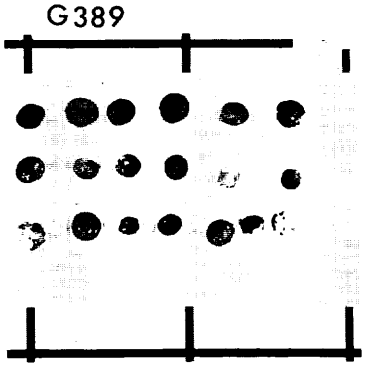

ST.722 FG52−1

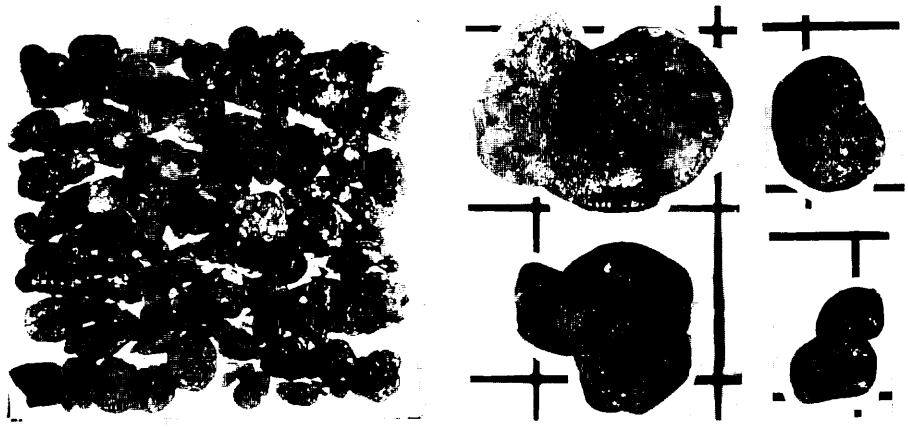

FG52−2

G391

ST.723 FG53−1

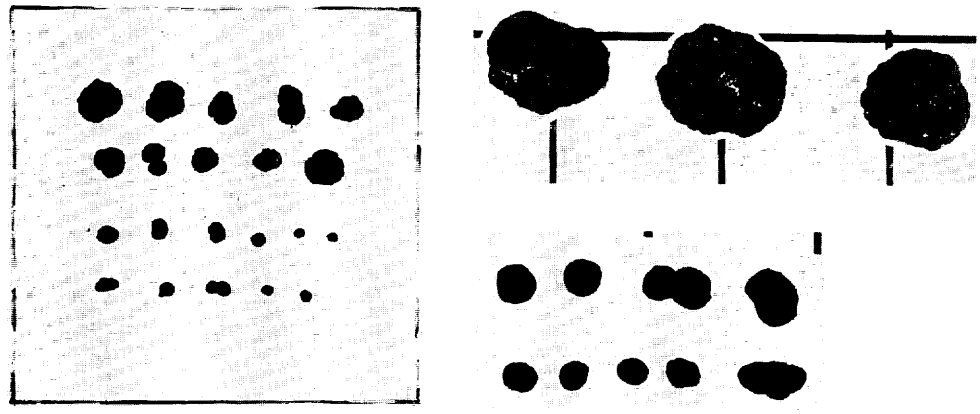

FG53−2

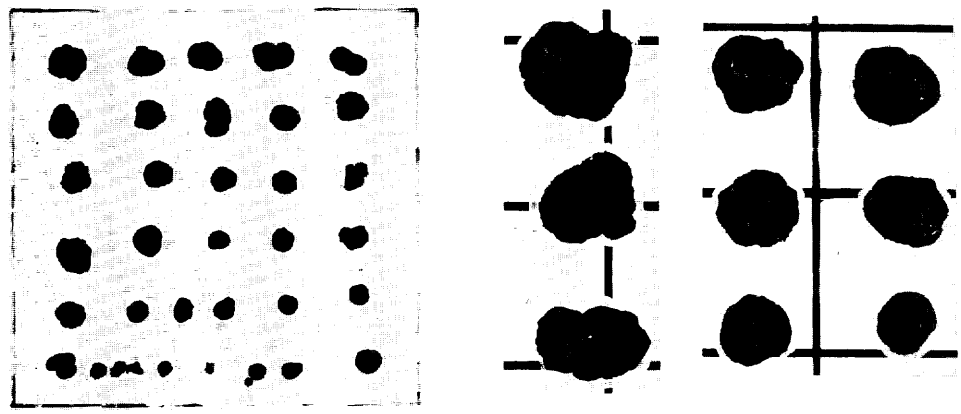

G392

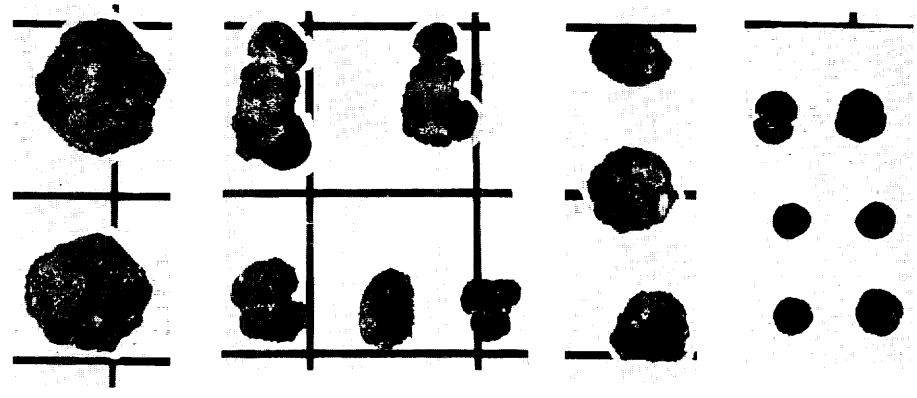

ST.724 FG54−1

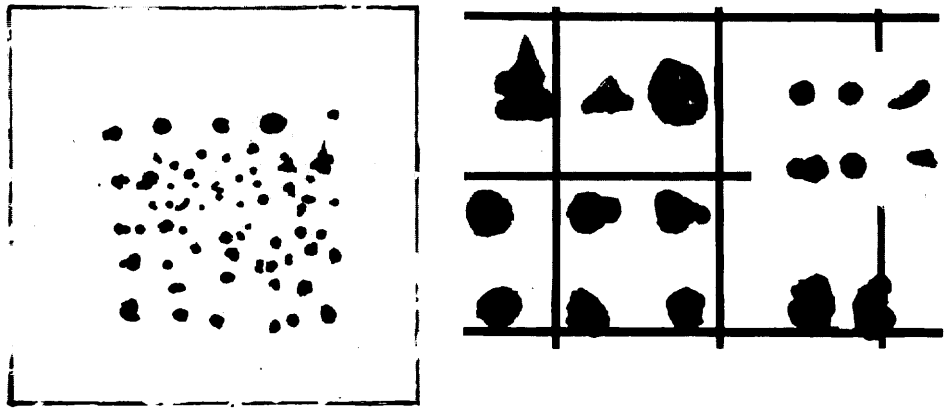

FG54−2

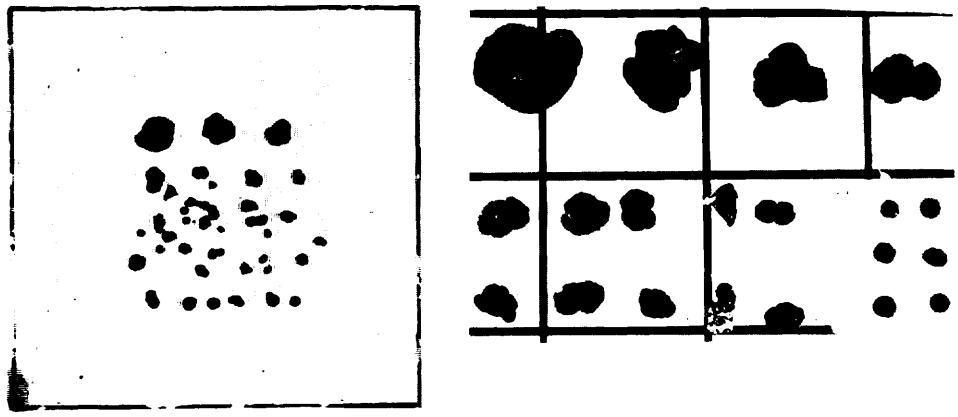

G393

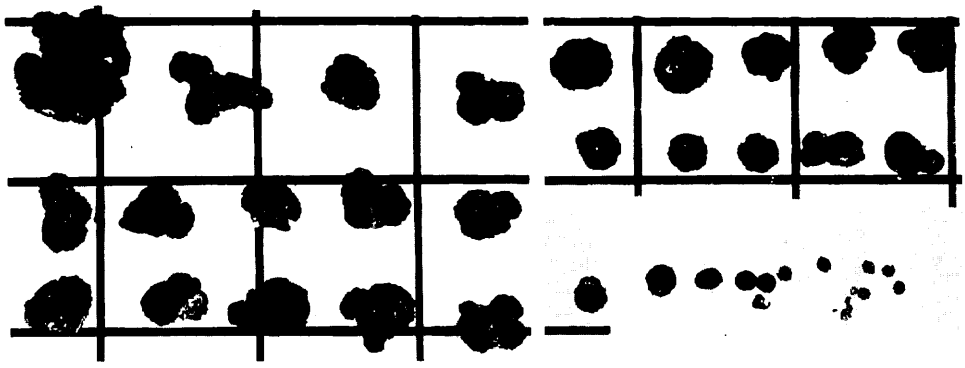

ST.725 FG55−1

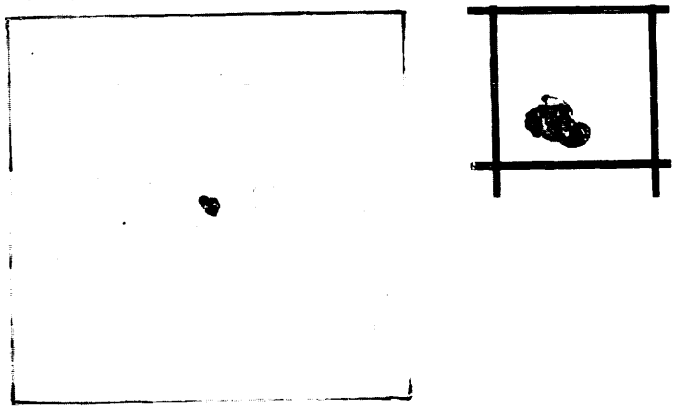

FG55−2

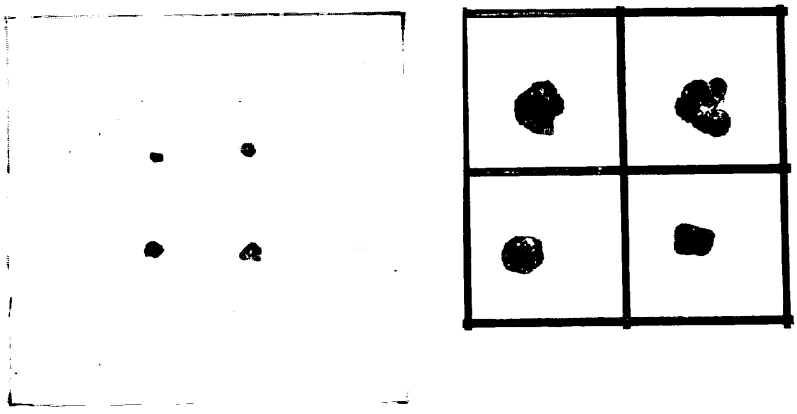

G394

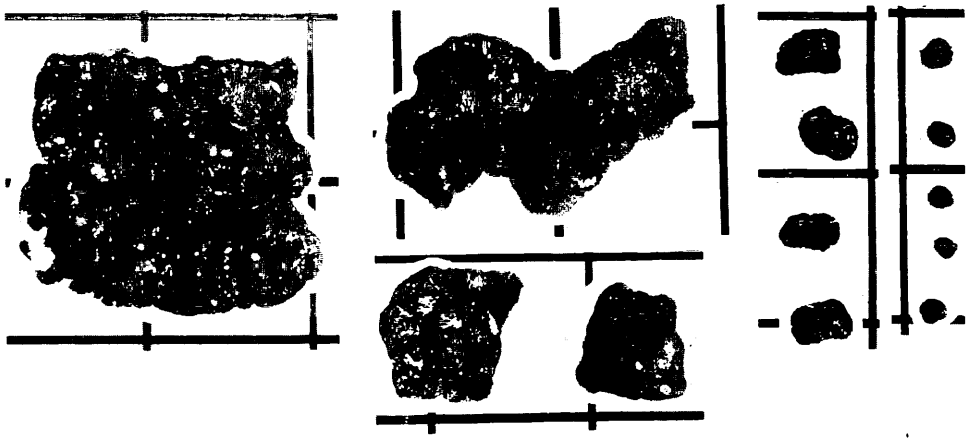

ST.727 G397

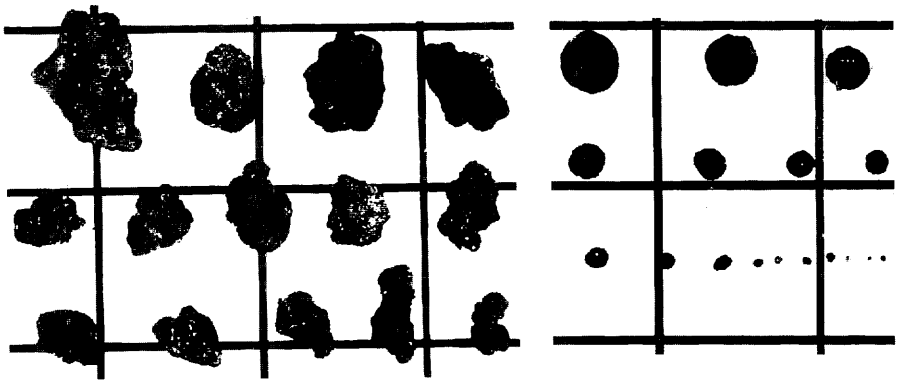

ST.728 FG60−1

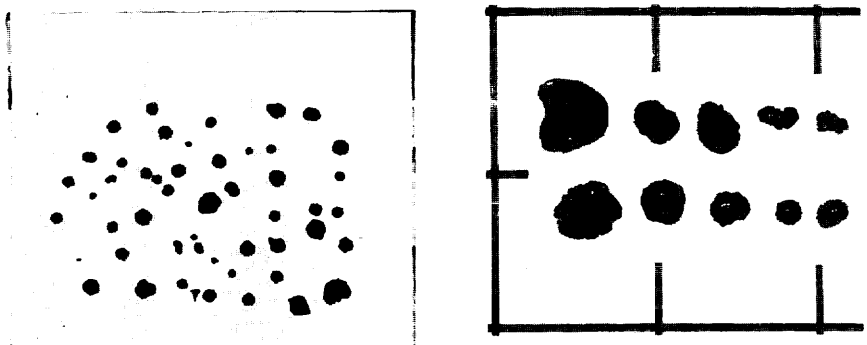

FG60−2

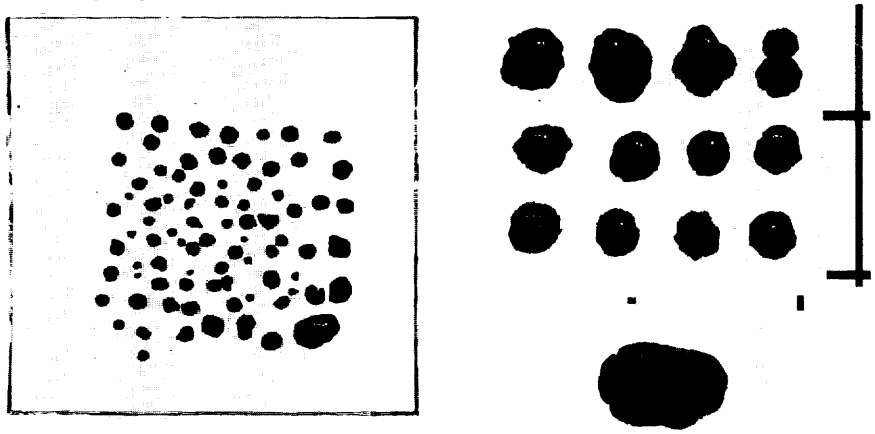

ST.729 FG61−1

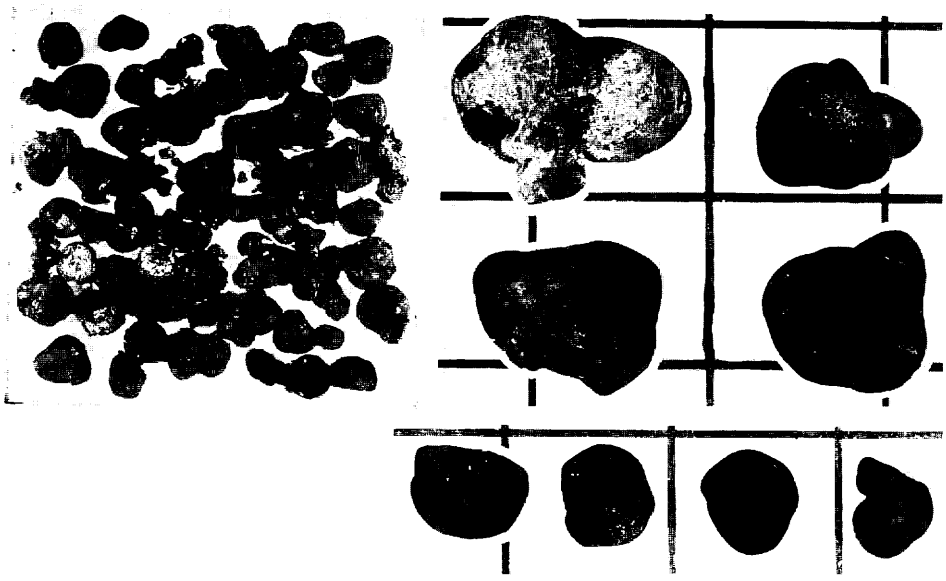

FG 61−2

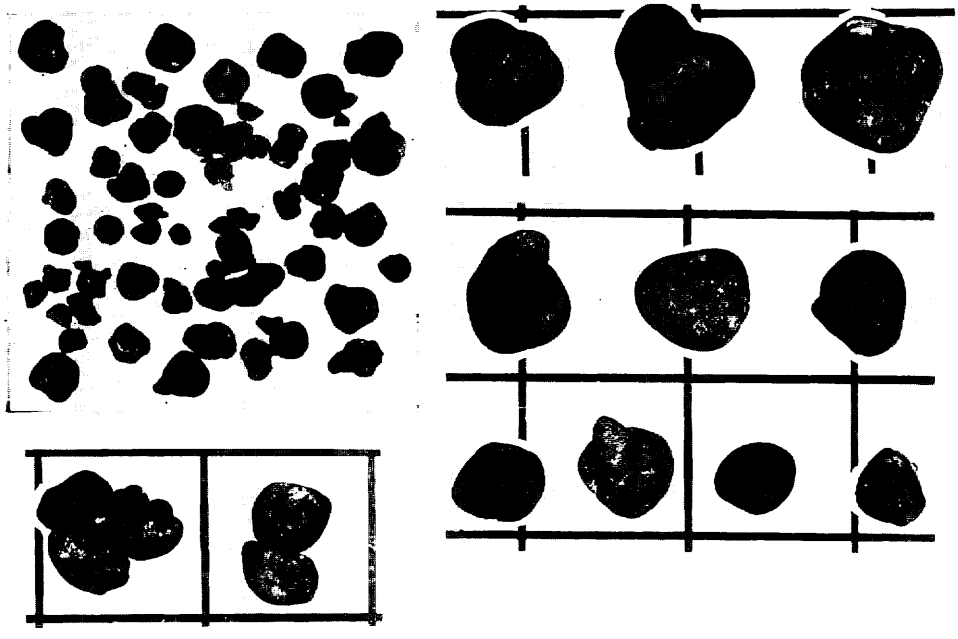

ST.730 FG62-1

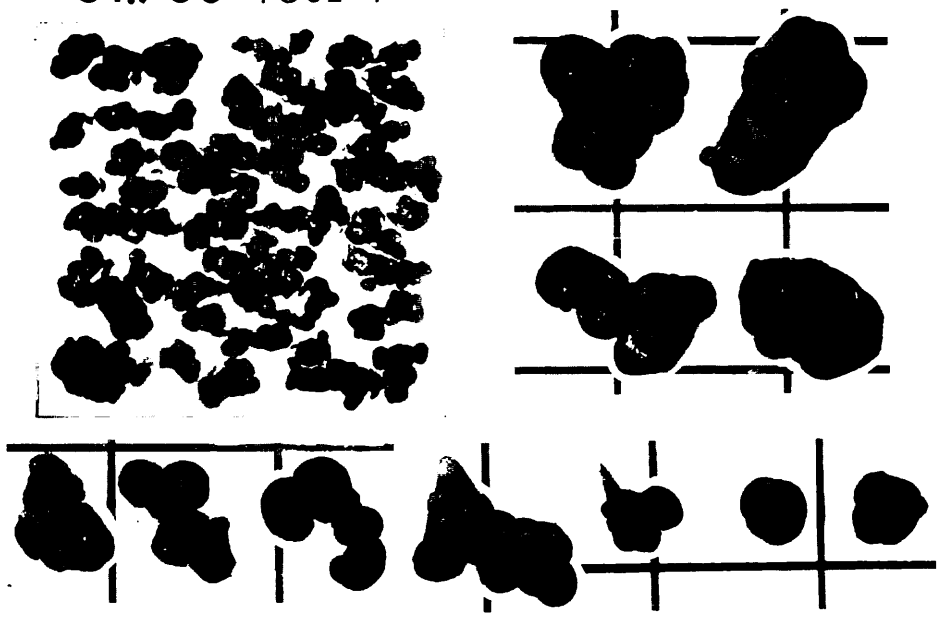

FG62-2

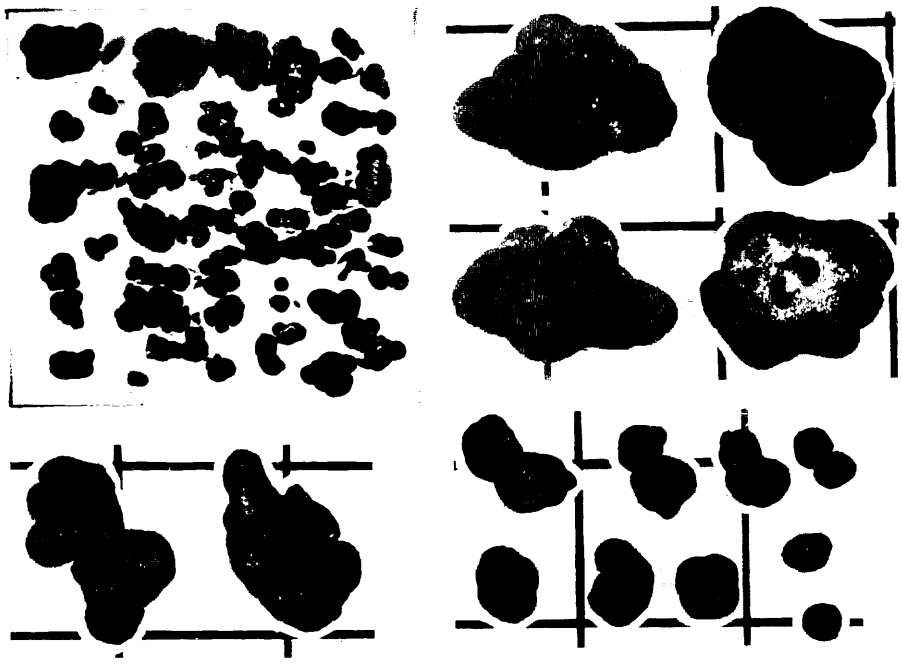

ST.732 FG64−1

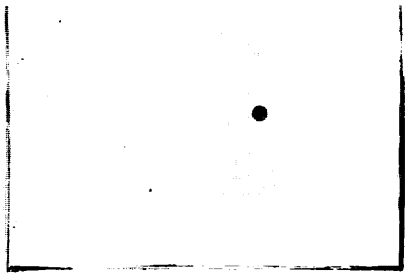

FG64−2

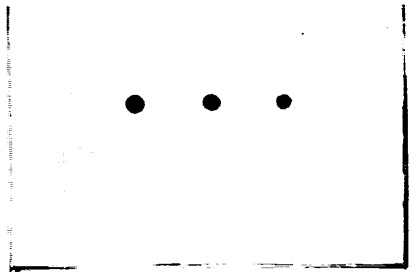

ST.733 FG65−1

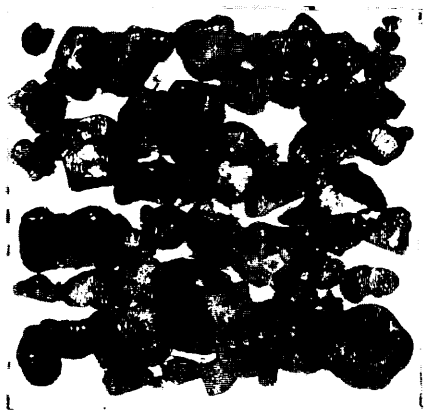

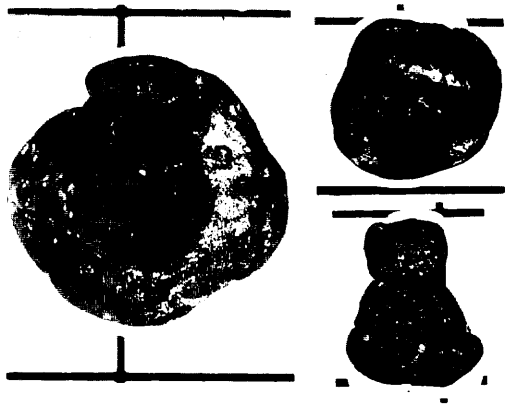

FG65−2

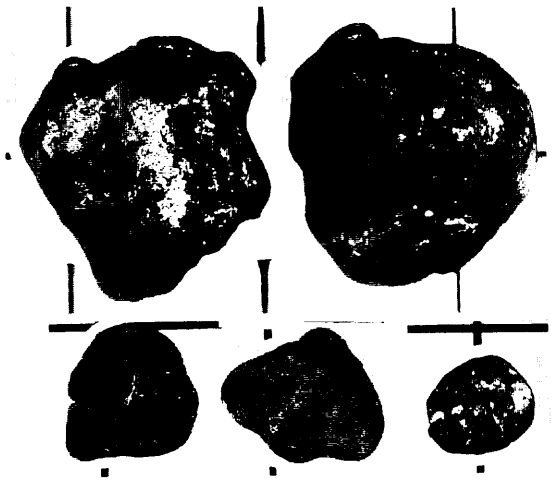

ST.734 FG66–1

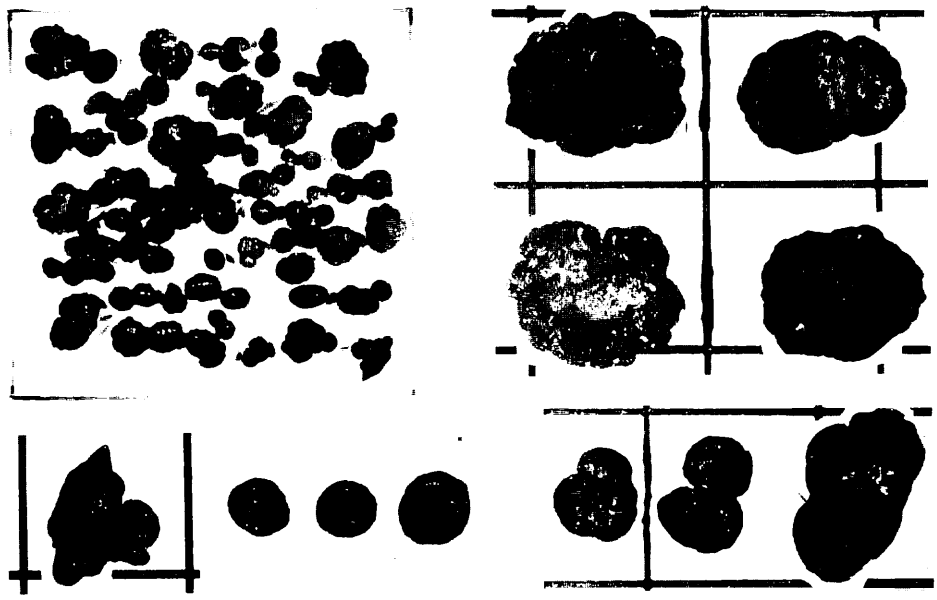

FG66–2

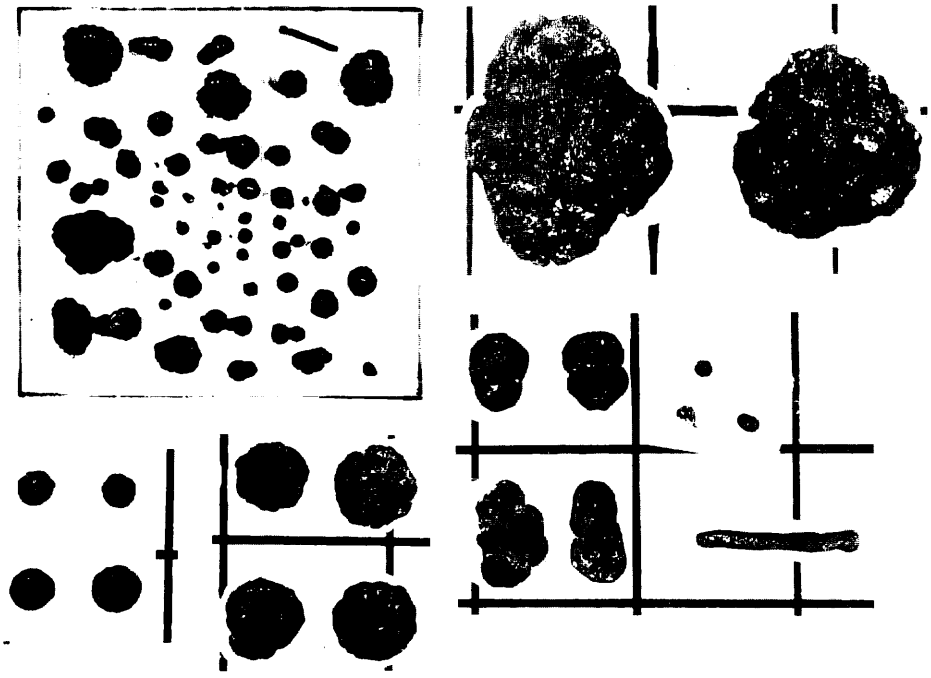

ST.735 FG67-1

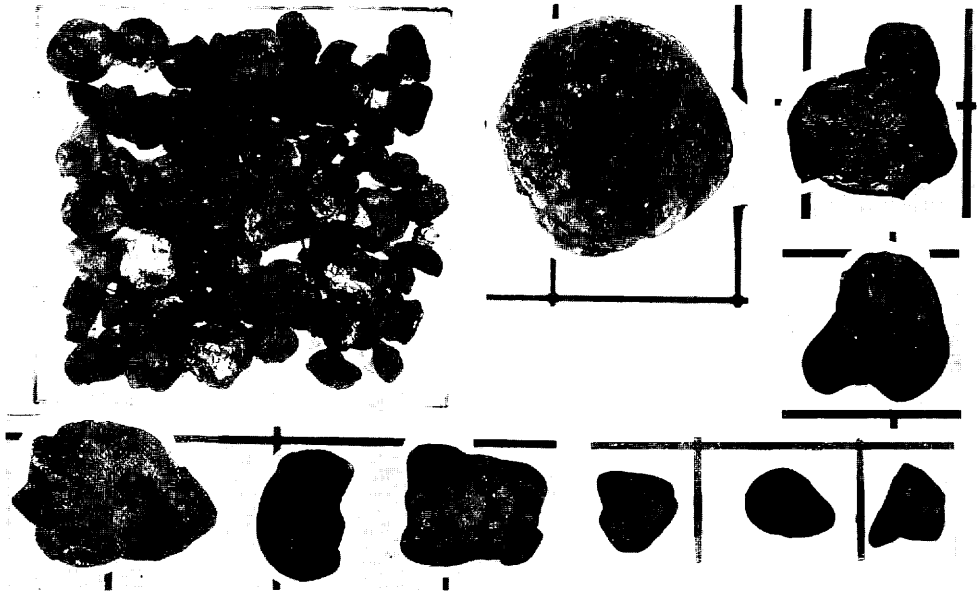

FG67-2

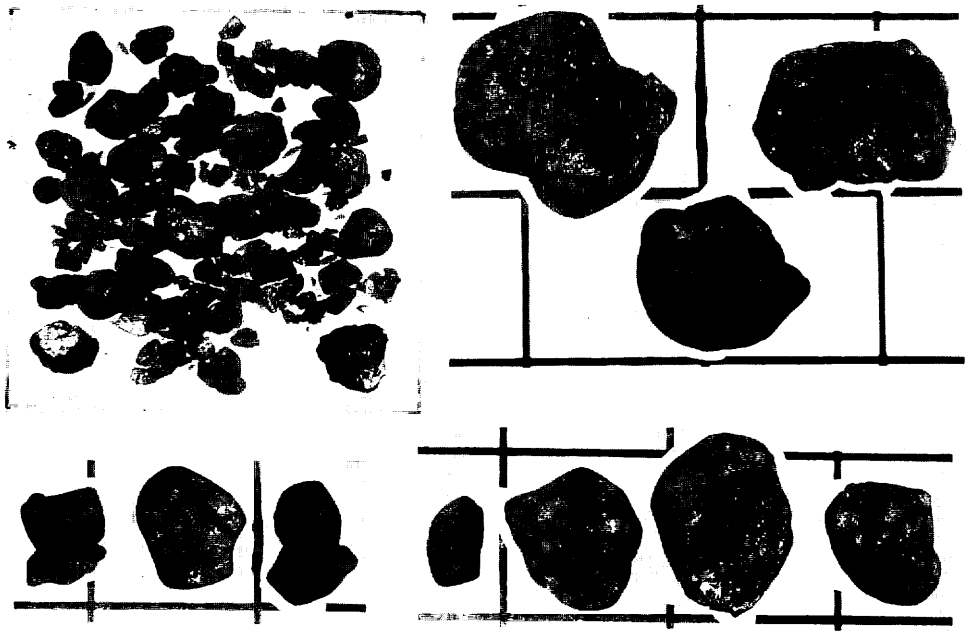

ST.736 FG68–1

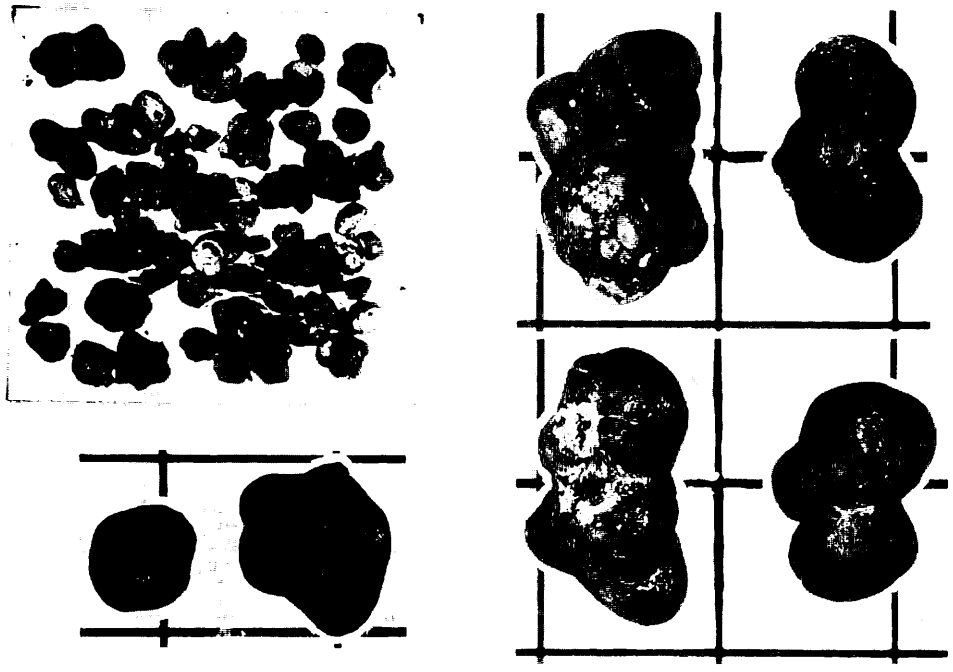

FG68–2

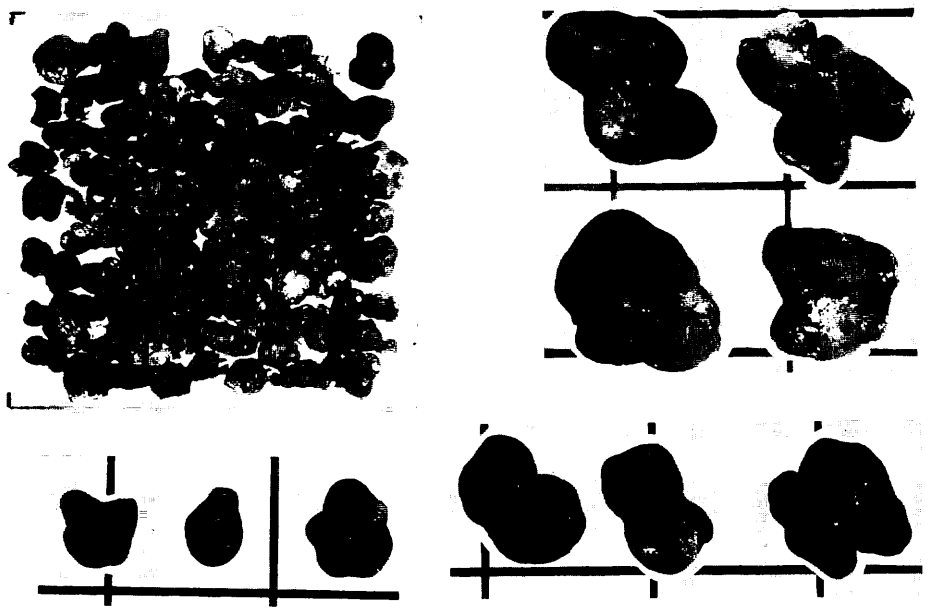

ST.737 FG69−1

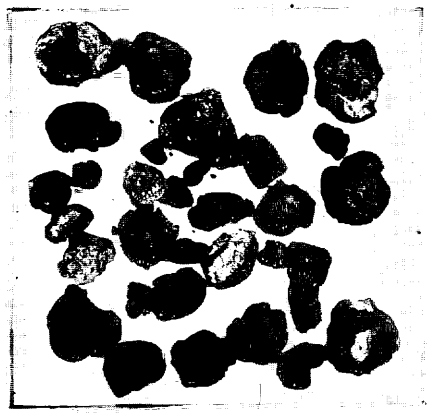

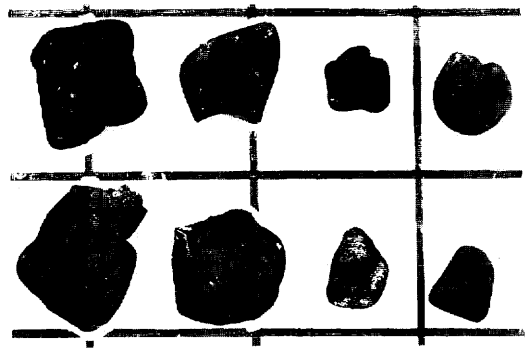

FG69−2

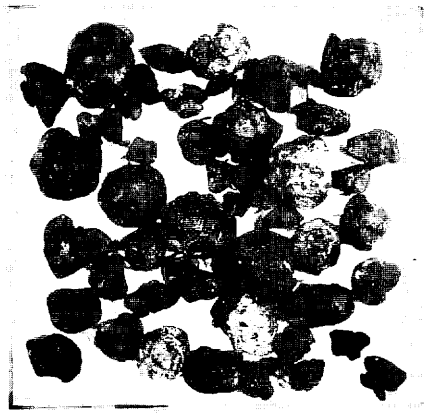

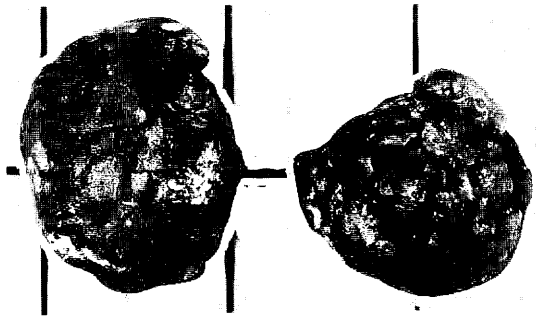

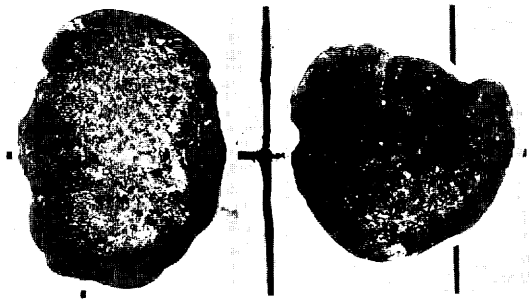

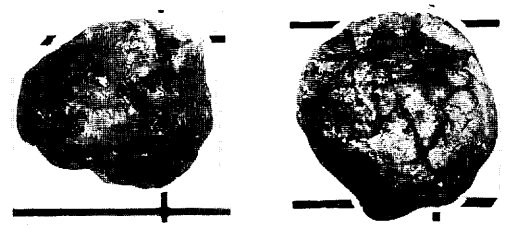

ST.738 FG70−1

FG70−2

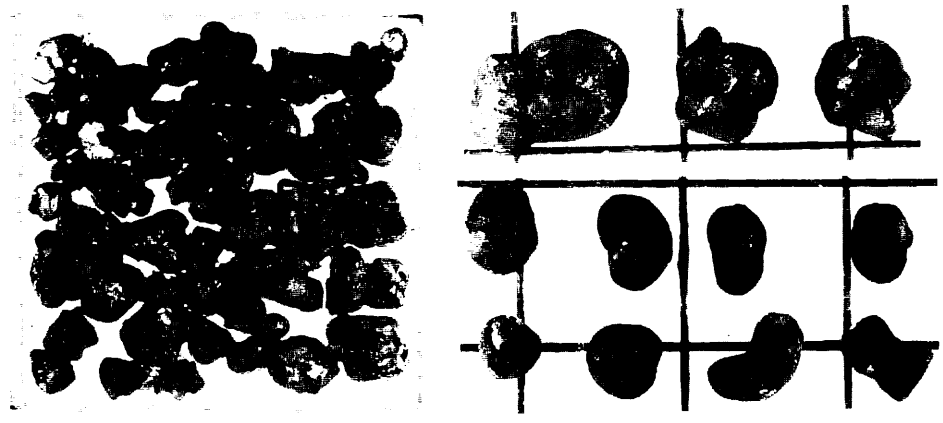

G402

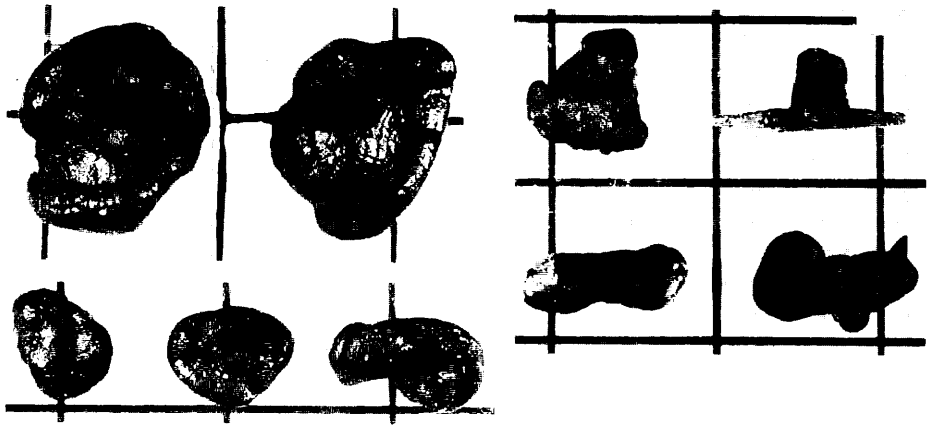

ST.739 FG72−1

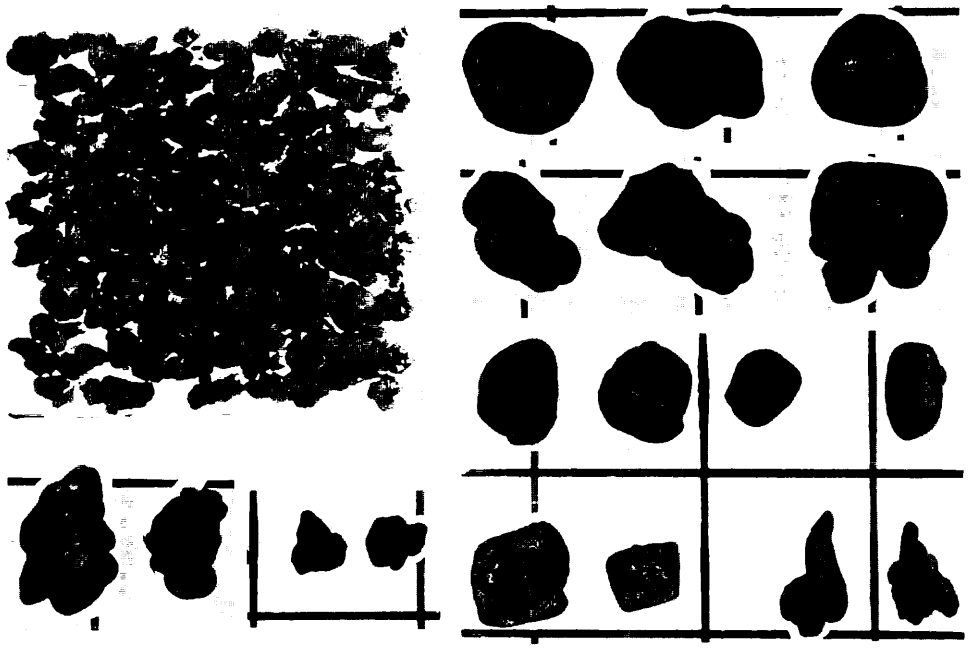

FG72−2

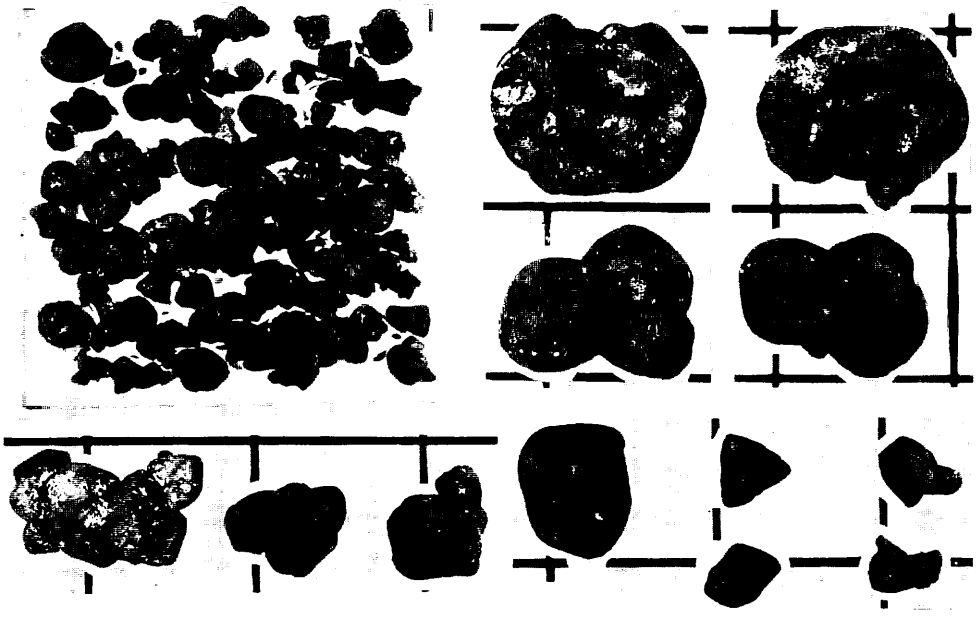

some olivine cristals are altered. According to the result data of the DSDP drilling, these basaltic rocks are thought to be those derived from the rock mass which constitutes the basement of the Magellan Rise.

Chert rocks were sampled from Sts. 706 and 711 (Fig. XIII–3(B)–2 and 3). These are thin plates of 2–5 cm thickness. Some are changed into agate. These rock fragments occur only on the surface of the bottom sediments.

Phosphorite rocks were sampled at St. 702 (Fig. XIII–3(B)–1). These are porous and rich in the remnants of biogenic activities. The horizon of the phosphorite is supposed to be correlative to that of the similar phosphorite found at St. 414 A-1 P67 of the GH76–1 cruise.

Reference

MORITANI, T., MARUYAMA, S., NOHARA, M., KINOSHITA, Y., OGITSU, T., and MORIWAKI, H. (1977) Description, classification, and distribution of manganese nodules. *In* A. MIZUNO and T. MORITANI (*eds.*), *Geol. Surv. Japan Cruise Rept.*, no. 8, p. 136–158.